An Innovative Multiparametric Sensor Design for Detecting Microplastics and Heavy Metals

Ekrem Kursad Dal[1,2,*], Adem Gunes[3], Recai Kilic[4]
[1]*Computer Programming, Cappadocia University,*
Mustafapasa Yerleskesi 50420, Urgup, Nevsehir, Turkiye
[2]*Graduate School of Natural and Applied Sciences, Electrical and Electronics Engineering, Erciyes University,*
Nuri- Zekiye Has Enstituler Binasi Fen Bilimleri Enstitusu 38039, Kayseri, Turkiye
[3]*Faculty of Agriculture, Erciyes University,*
Kosk Mahallesi Fuat Sezgin Caddesi No:12 38030 Melikgazi, Kayseri, Turkiye
[4]*Faculty of Engineering, Electrical and Electronics Engineering, Erciyes University,*
Merkez Kampus Talas Yolu, Melikgazi, Kayseri, Turkiye
[*]*ekrem.dal@kapadokya.edu.tr; ademgunes@erciyes.edu.tr; kilic@erciyes.edu.tr*

***Abstract*—Microplastics and heavy metals are materials that harm the environment and living organisms. Rapid detection enables their control or the identification of their sources. Conventional detection methods are expensive and require expert interpretation. The proposed sensor system detects these materials and evaluates their concentrations using a trainable multilayer perceptron algorithm. The system consists of twenty-two different light spectrum LEDs and eighteen narrow bandwidth photodiodes. The absorbance of incoming light and the shifted bandwidths in the spectrum can be evaluated by assessing multiparametric optical events. The study examines water samples containing eight different heavy metals, namely arsenic (As), cadmium (Cd), chromium (Cr), copper (Cu), mercury (Hg), nickel (Ni), lead (Pb), and zinc (Zn), along with three types of microplastics: melamine particles with a diameter of 8 µm, polystyrene particles with a diameter of 8 µm, and polystyrene particles with a diameter of 10 µm. Classification was performed in a concentration-dependent and concentration-independent manner. The system performance was improved by selecting features using the Ranker method of the InfoGain algorithm. Measurements were performed without applying any indicator chemicals. The system demonstrated high success in concentration-independent evaluation and acceptable concentration accuracy for heavy metals.**

***Index Terms*—Electro-optic devices; Hazardous materials; Multilayer perceptrons; Optical sensors; Water pollution.**

I. INTRODUCTION

The low recycling rate of plastic waste worldwide, industrial waste and unregulated disposal methods contribute significantly to environmental pollution [1]–[3]. Only a few centres and countries manage waste disposal or recycling in compliance with proper protocols. Waste discharged into oceans and seas can disintegrate and, through evaporation, enter the atmosphere, eventually returning to the ground via precipitation [4]. Consequently, fertile soils and clean natural water resources become contaminated [5], [6]. Microplastics and heavy metals are among the primary pollutants. This pollution is caused by disintegration, but is also exacerbated by industrial production. In some cases, microplastics and heavy metals coexist [7], [8]. Plastics coated with heavy metal-based paints can degrade into microplastics that carry heavy metals. Microplastics enhance the efficacy of the product or create the desired textures in industrial production, particularly in cosmetics and detergent products [8], [9].

Despite their known hazards, lead-containing paints, lead-based toys, water pipes, and mercury-containing fluorescent lamps are still used today [8], [10]. The accumulation of such pollutants negatively affects living organisms [11], [12]. In situations where they accumulate in the bodies of animals and humans, they harm beneficial microorganisms and promote the proliferation of harmful organisms [13]–[18].

Microplastics are formed by abrasion, degradation in nature, or intentional production of plastics for specific uses [8]. Microplastic refers to plastic particles smaller than five millimeters in size [19]. Microplastics a few millimeters in size are visible to the naked eye, making them less problematic for humans to avoid [8]. However, animals may still ingest these particles. For humans and animals, these nondigestible particles can accumulate in the body if not expelled [15]. Sharp or jagged microplastics can cause injuries and infections in the digestive system [1]. On the other hand, microplastics dissolved at the micron scale are difficult to detect with the naked eye. Due to their small size, they can penetrate tissues, causing tissue damage [15]. Their pigments and additives may include heavy metals and harmful chemicals [20]. Additionally, particles carrying microorganisms can pose a risk of spreading diseases [14].

The lack of recycling for batteries, metal objects, fluorescent lamps, and automobiles contributes significantly to heavy metal pollution [21]. General-purpose batteries containing nickel-metal hydride, nickel-cadmium, zinc-carbon, mercury, and lead-acid batteries can cause severe environmental damage when discarded improperly or in nature [21]. The heavy metals they contain are the primary problem. Although this pollution initially appears as soil contamination, rainwater can carry these metals to clean

Manuscript received 26 October, 2024; accepted 14 January, 2025.
The research was supported by the Erciyes University Scientific Research Projects Coordination Unit 317 under Grant No. FDK-2020-970.

water sources [22]. Heavy metal poisoning is known to have severe consequences. For example, Minamata syndrome, caused by the consumption of mercury-contaminated fish in Minamata Bay, Japan, and Itai-Itai disease, resulting from cadmium poisoning, are notable cases [23]. Heavy metal poisoning can lead to organ failure and death and can cause developmental deficiencies in children.

Microplastics are particulate contaminants that are typically detected and measured using micro-Fourier transform infrared spectroscopy (μ-FTIR) and μ-Raman instruments [24], [25]. Imaging-based techniques such as macroscopy, microscopy, multibeam optical microscopy, or fluorescence microscopy can visualise microplastics, though they cannot provide information about the type of plastic. Mass spectroscopy (MS) is among the methods for determining their chemical composition. Scanning electron microscopy (SEM) offers detailed information on the physical surface morphology of microplastics, but is insufficient for identifying their chemical composition [8]. Energy-dispersive X-ray spectroscopy (EDS) can provide surface chemical information, but is inadequate for internal structural analysis [26], [27]. Measurements with such instruments require evaluation by trained and skilled personnel, which limits operational capacity, introduces the potential for human error, and slows the process. Although portable handheld devices are available today, they are expensive [28]. It is essential to minimise sample preparation time and ensure rapid measurement and evaluation to identify sources of microplastic pollution. Additionally, increasing the number of measurement systems is necessary, requiring the devices to be more affordable. Even if such devices are available, evaluations will remain infeasible without adequate personnel. Research and developments targeting these challenges are ongoing.

Heavy metals can be detected using colour-changing chemicals or strips, flame atomic absorption spectrometry (Flame AAS), graphite furnace atomic absorption spectroscopy (GF-AAS), inductively coupled plasma mass spectrometry (ICP-MS), and inductively coupled plasma optical emission spectroscopy (ICP-OES) [29]–[33]. Strips and chemicals used for detection are typically single-use and their colour change responses can be inadequate when heavy metal concentrations are low [33]. Efforts have been made to develop electronic systems to detect colour changes in these chemicals [34]. However, the single-use nature of these chemicals can limit measurement continuity. Reducing the dependence on additional materials in such measurements offers significant advantages. Indicator chemicals, when stored improperly, can degrade over time. Moreover, the correct amount of indicator chemicals must be used for accurate results. Although measurement devices can provide precise results, they often require technical expertise for interpretation. Some laboratory instruments are now supported by artificial intelligence; however, the difficulty of performing on-site measurements and the prohibitive cost of these devices make them less accessible. Additionally, these devices often involve expensive calibration processes and consumables. Sometimes, sample pretreatment is required before measurements can be taken with these instruments.

This study presents an innovative liquid sample sensor system capable of on-site measurement and accurately classifying microplastics and heavy metals without requiring special sample preparation. The system scans narrow bands within ultraviolet, visible, and near-infrared spectra. It can optimise the selection of light sources and narrow bands to correctly classify measured samples, thus determining the necessary light source, narrow-band optical filter, or photoreceptor based on the specific problem. For the testing of the system, microplastic samples consisting of 8 μm polystyrene, 10 μm polystyrene, and 8 μm melamine were prepared at concentrations ranging from 1 μl to 10 μl in water. Additionally, arsenic (Ar), cadmium (Cd), chromium (Cr), copper (Cu), mercury (Hg), nickel (Ni), lead (Pb), and zinc (Zn) were dissolved in water at concentrations of 25 ppm, 50 ppm, and 100 ppm as heavy metal samples.

Materials were identified without isolating parameters such as absorbance, spectral shift, and scattering. These optical phenomena are filtered and measured as single parameters in conventional spectrophotometry devices. For instance, a visible spectrum spectrophotometer, which uses a light source in the visible region, measures the absorption of incoming and transmitted light based on the Beer-Lambert law. However, scattering events are not typically evaluated as a parameter in these devices, as the measurement results are expected to remain unaffected by scattering. In our system, scattered light is absorbed by a black surface, leading to attenuation of the central beam. In samples containing phosphors, ultraviolet radiation can cause scattering at different wavelengths. Similarly, Raman scattering can result in shifts that produce emissions at various wavelengths. These shifts cause certain photodiodes to detect lower light intensities, while others detect higher intensities, depending on the light source. The optical differences inherent to the materials form the optical characteristics of the sample. In Section II, studies related to our work are presented and the innovative aspects of the study are emphasised. Section III discusses the structure and detection mechanism of the sensor system. Section IV demonstrates the classification of samples using a multilayer perceptron and the impact of feature selection on the system's performance. Section V presents the results and explores alternative system designs and potential application areas.

II. RELATED WORKS

In this section, the vulnerabilities and scope of the existing literature are analysed, culminating in a summary of the research studies presented in Table I. When the relevant studies are examined, no portable device or system has been found other than laboratory devices that can detect both microplastics and heavy metals at the same time. Laboratory devices have general use, not problem-orientated use, and the evaluation of the results requires technical knowledge. In addition, they are not efficient in terms of real-time applications because they are expensive. For this reason, there is a need for a simple, problem-orientated, customisable, nondestructive sensor suitable for taking measurements. In the literature, the available devices are primarily laboratory instruments, or apparatuses and probes specifically designed for laboratory applications [24]–[27]. In some studies, artificial intelligence techniques have been utilised to process data obtained from these laboratory devices [35]. Given that the term microplastic refers to

particles smaller than 5 mm, studies focussed exclusively on micron- or nano-sized particles, which are invisible to the naked eye, are considered separately. Detection methods based on image processing or camera-based systems are predominantly used to identify larger particles [36]. For smaller particles, analyses involving interference patterns or scattering phenomena are more commonly used [37]. The use of chemical indicators for heavy metal detection has been extensively reported in many studies [34], [38], [39].

The primary objective of the present study is to enable detection without the need for additional processes or chemical reagents other than filtering large particles. Furthermore, it aims to classify concentration levels as low, medium, or high on the basis of quantitative measurements.

TABLE I. RELATED WORKS.

Related Work	Indicator Usage	HM Detection	MP Detection	Portable	AI/ML Usage
[3]	No	No	Yes	No	Yes
[40]	No	No	Yes	No	Yes
[41]	Yes	No	Yes	No	No
[37]	No	No	Yes	No	No
[34]	Yes	Yes	No	Yes	No
[38]	Yes	Yes	No	Yes	No
[42]	Yes	Yes	No	Yes	Yes
This Study	No	Yes	Yes	Yes	Yes

Note: HM – Heavy Metal, MP – Microplastic, AI/ML – Artificial Intelligence/Machine Learning.

III. MATERIALS AND METHODS

The optical phenomena that occur during sample detection are distinctive features of the material. These distinguishing characteristics may vary depending on the type of substance being detected. Factors such as particle size, whether the substance is dissolved in the liquid, morphology, and molecular or elemental structure influence the optical characteristics. In cases where the material consists of particles and no dissolution occurs, it is well known that scattering effects are pronounced. Even in such situations, both elastic and inelastic scattering can be observed. On the other hand, in dissolved substances, the absorbance provides information about the type of material. Material detection can also be achieved by examining changes in optical characteristics induced by excitation through high-energy photons, heat, magnetic fields, electric fields, or chemical reactions.

When a light beam passes through a material, it undergoes a loss, typically converting into another form of energy, such as heat. This phenomenon is known as absorption. Absorption varies depending on the structure of the material, with specific light wavelengths absorbed while others are transmitted more effectively. This behaviour is influenced by the composition of the material, the surface morphology, additives, and pigments. The amount of absorbed light is described by the Beer-Lambert law

$$A = \varepsilon c l. \tag{1}$$

According to the equation, A represents absorbance, ε denotes the molar absorption coefficient, c is the molar concentration, and l represents the path length in centimeters (cm). Spectrophotometer cuvettes typically have a path length of one centimeter. Equation (2) provides an alternative expression for absorbance

$$A = \log_{10} \frac{I_0}{I}. \tag{2}$$

In (2), I_0 represents the incoming monochromatic light and I represents the light transmitted through the material. Since the light sources used in the system are LED-based and lack filters, obtaining monochromatic light is not possible. Instead, the absorption of light across a spectral range, based on the type of material, is made possible by monitoring the transmitted light across multiple spectral regions. This process is performed in spectrophotometer devices by dispersing light into its spectra, typically observed using line-type charge-coupled device (CCD) sensors. These devices include optical arrangements to ensure that light of the same wavelength reaches the same photodiode, regardless of changes in the angle of incoming light.

In these sets of equations, assuming a fixed cuvette path length of 1 cm and a constant incident light intensity, the absorbed light is proportional to the molar absorption coefficient and concentration of the material. The molar absorption coefficient also varies depending on the wavelength of the incident light. Since the measurements are evaluated using machine learning, the analysis was conducted under fixed conditions by measuring transmitted light (transmittance).

For particulate and undissolved samples, not only absorbance but also diffraction and scattering phenomena occur during the determination of the type and concentration of the material. Diffraction is the bending and spreading of light in different directions when it passes through apertures smaller than its wavelength or encounters an obstacle. Depending on the size of the obstacle, diffraction can be described using Fraunhofer Diffraction or Fresnel Diffraction. The relationship between the diffraction angle, wavelength, and obstacle size is given in (3)

$$\theta = \frac{\lambda}{d}. \tag{3}$$

In this equation, λ represents the wavelength of light and d denotes the size of the aperture or obstacle the light encounters. As the wavelength of light decreases, the diffraction angle θ also becomes smaller. Thus, light with shorter wavelengths undergoes a lesser amount of diffraction.

Moreover, irregularities, roughness, nanostructures and microstructures, or cracks on the surface of an object can also cause diffraction. These features are collectively called surface morphology, which describes the structural and geometric characteristics of the surface of an object. The surface morphology significantly influences the scattering and diffraction characteristics of light.

Another optical phenomenon that occurs is scattering. Scattering typically arises from the interaction of incoming light with material and appears in various directions depending on the surface morphology. For particles of micron size, Mie and Raman scattering are commonly observed. Mie scattering refers to elastic scattering caused by interactions between light and particles with sizes comparable to or larger

than the wavelength of the light. In elastic scattering, the energy and wavelength of light remain unchanged, but the light is scattered in all directions. Mie scattering is calculated using a spherical harmonic series. The fundamental equation for Mie scattering, expressed through the solutions of Maxwell's equations in spherical coordinates, is presented in (4)

$$S(\theta)=\sum_{n=1}^{\infty}(2n+1)(a_n\pi_n(\cos\theta)+b_n\tau_n(\cos\theta)). \quad (4)$$

In this equation, a_n and b_n represent the Mie scattering coefficients, $\pi_n(\cos\theta)$ and $\tau_n(\cos\theta)$ denote the spherical harmonic functions, and n is the series expansion index. This formula calculates the angular distribution and intensity of light interaction with particles in Mie scattering. Monochromatic light forms a uniform ring pattern under the influence of these coefficients. However, when broad-spectrum light sources (e.g., LEDs) are used, these rings split into spectral distributions, creating a rainbow-like appearance. The scattering of different wavelengths of light at varying angles explains this phenomenon.

Raman scattering, on the other hand, is an inelastic scattering phenomenon caused by interactions with micron-sized particles. In Raman scattering, the material absorbs some of the energy from the incoming light, resulting in scattered photons with altered frequencies. This process is described by the Raman shift, which provides insight into the chemical and molecular composition of the sample. The Raman shift is expressed in (5)

$$\Delta\nu=\nu_i-\nu_s. \quad (5)$$

In the given equation, $\Delta\nu$ represents the Raman shift, ν_i denotes the frequency of the incident photon, and ν_s denotes the frequency of the scattered photon. Raman spectroscopy analyses the chemical structures of microplastics on the basis of the frequency shifts that occur.

As a result of these optical phenomena, it has been observed that Mie scattering is predominant in particulate and undissolved materials. In the proposed system, the rainbow-like scattering caused by the LED light sources is blocked by black surfaces, resulting in attenuation of the direct radiation. Narrow-spectrum photodiodes detect this attenuation for different spectral light sources, providing a multiparameter spectral characteristic specific to the material. Although it is difficult for humans to evaluate directly, the spectral characteristic data generated in this manner can be effectively analysed using machine learning algorithms.

With its multilayer structure, the multilayer perceptron algorithm is an artificial neural network capable of learning complex relationships between data and desired outputs. It is particularly widely used in classification and regression analyses. The algorithm consists of three main layers: input, hidden, and output. First, the data are fed into the input layer and processed through the hidden layers. In each layer, the neurons multiply their input by certain weights and sum them. This sum is then passed through an activation function. The activation function enables the model to learn nonlinear relationships. Standard activation functions include sigmoid, rectified linear unit (ReLU), and tanh. The model learning process is carried out using a method called backpropagation, in which the difference (amount of error) between the model predictions and the actual values is minimised by updating the model weights. This is typically achieved through the gradient descent algorithm. During training, the model reduces errors by adjusting its weights, thereby improving its ability to make accurate predictions.

IV. EXPERIMENTS

The present study proposes a system to measure the spectral characteristics of samples using 22 LED-type light sources and 18 narrow-band photodiode sensors. The data obtained were analysed using the multilayer perceptron (MLP) algorithm. The block diagram of the system is presented in Fig. 1.

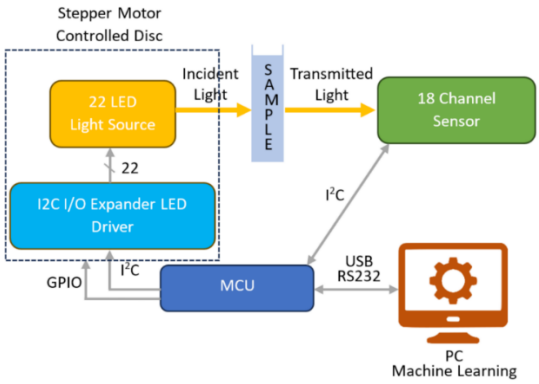

Fig. 1. Diagram of the system.

A. Setup

The light sources for material detection were selected from commonly available LEDs rather than specially manufactured LEDs for laboratory work. According to the information provided by the vendors, 22 different light sources were used; however, these data are known to be not entirely reliable. For this reason, the spectra of these 22 LEDs were measured and analysed using a spectrometer. The primary purpose of selecting these LEDs in this way is to examine the LEDs commonly used on the market and their applicability in material detection.

The system used 18 narrow-band photodiodes and SparkFun Triad Spectroscopy Sensor modules containing AS72651, AS72652, and AS72653 sensors with built-in analogue-to-digital converters. The spectral response of the photodiodes used in the sensors is shown in Fig. 2.

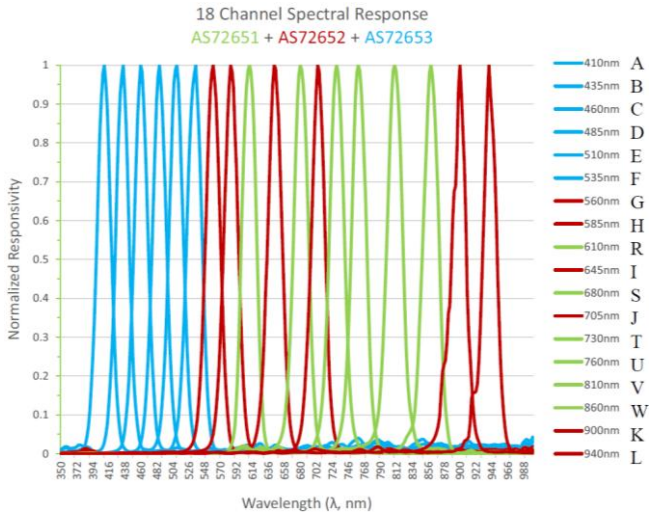

Fig. 2. Spectral response of AS7265x photodiode channels [43].

The light spectrum of the 22 LEDs used is shown in Fig. 3. Because of the three wide-spectrum LEDs (cool white, warm white, and pink) in the system, the gaps that may occur in the visible spectrum are closed. Light spectra were measured with an ocean optics flame spectrometer.

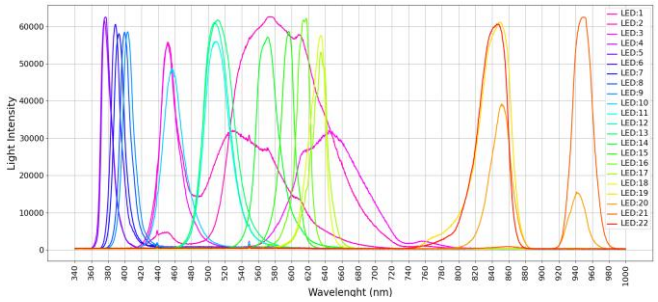

Fig. 3. Light spectrum of the LEDs.

The SparkFun triad spectroscopy sensor module is designed for reflective measurements; however, modifications were made to enable the module to measure incoming light. Since the sensor module board is red, parts of the sensor, other than the photodiodes, were masked using black PVC tape. The LEDs on the module were disabled to ensure that only incoming light could be measured. As these three sensor boards were placed in discrete positions and the light acceptance angle of the sensor was insufficient for measurements, the incoming light was diffused onto the sensor surface twice using a diffuser film. These procedures were carried out within an enclosure to reduce ambient noise in the measurements. The setup with the enclosure is shown in the measurement system in Fig. 4.

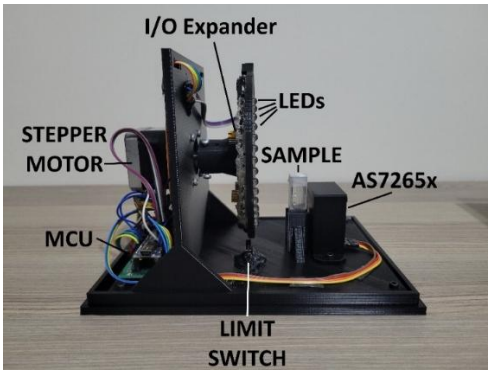

Fig. 4. The measurement setup.

In the system, a stepper motor-based movement mechanism is used along with LED light sources mounted on a disk, and their corresponding driver is employed to select the light source. Once the appropriate position of the LED is adjusted by using the stepper motor, the light source is turned on for measurement. After the measurement, the light source is turned off, and the system moves to the next position of the LED light source.

B. Processing Data

Three hundred ninety-six light data points were obtained by measuring samples after passing 22 different LED beams through a cuvette using 18 distinct narrow-band photodiodes. These data were transferred to a computer via a USB/RS232 converter and recorded in tables. Preliminary examination and labelling processes were applied to the recorded data. To avoid erroneous measurements, the data were collected through 10 repeated measurements. The data obtained were labelled with headings and added to a comprehensive table containing all data. Six tables were derived from this main table: heavy metal with concentration, microplastics with concentration, combined data with concentration, and their concentration-independent versions. In concentration-dependent classification, the primary objective was to observe whether classification could be performed based on pollution levels, thus evaluating the functionality of the system as a pollution measurement device. In the concentration-independent case, the focus was on determining the accuracy of the system in detecting the presence of these pollutants. During the training of concentration-independent classes, samples with varying concentrations were used for training and testing. The primary purpose of the two distinct evaluations is to determine the limits of the system's capability.

The data set contains data that could potentially contribute to misclassifications. This issue arises because the system's spectral range is not tailored to the specific characteristics of the samples. Therefore, feature selection algorithms were also applied to the data. The InfoGain algorithm with the Ranker method was used as the feature selection approach. The impact of selecting the top 10 and 20 features on the classification results was examined.

The data were evaluated using the MLP algorithm, a type of multilayer artificial neural network. This algorithm is employed as a machine learning method for analysing nonimage data. Due to its hidden layers and the inclusion of multiple neurons, MLP is categorised as a deep learning algorithm. The WEKA software was used to train the network and analyse the data [44]. The parameters used to train the MLP algorithm are shown in Table II.

TABLE II. MLP TRAINING PARAMETERS.

Parameter	Value
Hidden Layer	Automatic
Learning Rate	0.3
Momentum	0.2
The Number of Epoch	500
Numbers Decimal Places	2
Validation Threshold	20

Two different testing methods were used while processing data with the MLP algorithm: 10-fold cross validation and data division into training and testing subsets. This approach ensured confidence in the accuracy of the results. The test data were obtained by randomly separating 33.33 % of the entire data set, ensuring that this subset was excluded from the training process. The selection of these test data was performed by a computer using a random function.

V. RESULTS

The system data were evaluated using the multilayer perceptron (MLP) algorithm. Two distinct methods were applied to ensure impartiality in the evaluation: 10-fold cross validation and data separation into training and testing subsets. The data were analysed on the basis of their concentration and pollution type and independently of concentration, focussing solely on pollution type classification.

Table III presents the concentration-dependent classification accuracy success results for pollutants.

TABLE III. CLASSIFICATION ACCURACY SUCCESS RESULTS BASED ON CONCENTRATION DEPENDENCE.

	Heavy Metals (24 Class)	**Microplastics (30 Class)**	**Combined Data (54 Class)**
Cross Validation	76.9444 % (Fig. 9)	48.6667 % (Fig. 7)	47.5309 % (Fig. 5)
Cross Validation (Top 10 Feature Selected)	82.0833 % (Fig. 21)	56.2222 % (Fig. 19)	54.9383 % (Fig. 17)
Cross Validation (Top 20 Feature Selected)	81.3889 % (Fig. 33)	66 % (Fig. 31)	64.5679 % (Fig. 29)
66 % Training, 33 % Test Split	63.3333 % (Fig. 10)	46.3333 % (Fig. 8)	43.5185 % (Fig. 6)
66 % Training, 33 % Test Split (Top 10 Feature Selected)	78.75 % (Fig. 22)	48.6667 % (Fig. 20)	45.7407 % (Fig. 18)
66 % Training, 33 % Test Split (Top 20 Feature Selected)	73.75 % (Fig. 34)	55.3333 % (Fig. 32)	55.5556 % (Fig. 30)

The confusion matrices corresponding to the reported accuracy percentages are presented as figures. Confusion matrices showing the detailed classification results of the result are also given with the success percentage. Confusion matrices show the classification results as actual (rows-vertical axis) and predicted (columns-horizontal axis). In the confusion matrix, elements from the periodic table were used as labels for heavy metals. For microplastics, “ps” denotes polystyrene, “me” denotes melamine, and the letter “u” represents microns. For example, in microplastic samples, the expression “ps_10u_5ul” indicates the presence of spherical polystyrene microplastics with a diameter of 10 micrometers, found in five microliters within a 2.5 ml sample. Similarly, in heavy metal samples, the expression “50ppm_cd” indicates the presence of cadmium at a concentration of 50 parts per million (ppm). In the independent evaluation of concentrations, the quantity was considered irrelevant; only the type of microplastic or heavy metal present was taken into account. Within the concentration-based measurements, the classification accuracy of heavy metals was higher than that of microplastics. The lowest classification accuracy was observed in the combined data set. For heavy metals, an increase in concentration leads to a higher absorbance, whereas for particulates, both the absorbance and scattering effects increase. In particular, at low concentrations, the measurement of scattering-dependent transmittance poses significant challenges.

Table IV shows the classification accuracy success results of the measurements independent of concentration. For each percentage of accuracy reported, the corresponding confusion matrix is presented as a figure. It was found that the detection of microplastics independent of concentration could achieve high accuracy rates. Classification based on material type and size yielded accuracy levels that were deemed acceptable. Concentration-independent evaluation generally improved many outcomes.

TABLE IV. CLASSIFICATION ACCURACY SUCCESS RESULTS INDEPENDENT OF CONCENTRATION.

	Heavy Metals (8 Class)	**Microplastics (3 Class)**	**Combined Data (11 Class)**
Cross Validation	86.25 % (Fig. 15)	97 % (Fig. 13)	72.0988 % (Fig. 11)
Cross Validation (Top 10 Feature Selected)	81.1111 % (Fig. 27)	95 % (Fig. 25)	85.6173 % (Fig. 23)
Cross Validation (Top 20 Feature Selected)	91.9444 % (Fig. 39)	98 % (Fig. 37)	90.1235 % (Fig. 35)
66 % Training, 33 % Test Split	82.0833 % (Fig. 16)	97 % (Fig. 14)	87.5926 % (Fig. 12)
66 % Training, 33 % Test Split (Top 10 Feature Selected)	83.3333 % (Fig. 28)	95 % (Fig. 26)	85.3704 % (Fig. 24)
66 % Training, 33 % Test Split (Top 20 Feature Selected)	93.75 % (Fig. 40)	97.3333 % (Fig. 38)	91.2963 % (Fig. 36)

Feature selection contributed positively to the overall improvement of the results. Comparable results were obtained in both cases where the data were evaluated using cross validation and when split into training and test data sets. The scoring results of the top 10 features, obtained through feature selection applied to concentration-dependent classes, are presented in Fig. 41. The features corresponding to these scores are provided in the example data set in Table V.

a	b	c	d	e	f	g	h	i	j	k	l	m	n	o	p	q	r	s	t	u	v	w	x	y	z	aa	ab	ac	ad	ae	af	ag	ah	ai	aj	ak	al	am	an	ao	ap	aq	ar	as	at	au	av	aw	ax	ay	az	ba	bb	<-- classified as
19	1	1	1	0	1	0	1	0	0	0	0	0	0	0	0	0	0	0	0	1	0	0	0	0	0	0	0	0	0	0	0	0	1	2	1	0	0	0	0	0	0	0	0	1	0	0	0	0	0	0	0	0	0	a = ps_8u_1ul
0	9	4	4	4	0	0	0	0	0	0	0	0	2	0	0	0	0	0	0	0	0	0	0	2	1	0	0	0	0	0	0	0	0	0	0	0	0	0	0	0	0	2	1	0	0	0	0	0	1	0	0	0	0	b = ps_8u_2ul
0	6	11	6	2	0	0	0	0	0	0	0	0	0	1	0	0	0	0	0	0	2	0	0	0	0	0	0	0	0	0	0	0	0	0	0	0	0	0	0	0	0	1	0	0	0	0	0	0	0	0	1	0	0	c = ps_8u_3ul
3	2	6	9	3	0	0	1	1	0	0	0	0	0	1	1	0	0	0	0	0	2	0	1	0	0	0	0	0	0	0	0	0	0	0	0	0	0	0	0	0	0	0	0	0	0	0	0	0	0	0	0	0	0	d = ps_8u_4ul
0	3	2	5	14	0	1	0	1	0	0	0	0	1	0	0	0	0	0	0	0	0	0	1	0	1	1	0	0	0	0	0	0	0	0	0	0	0	0	0	0	0	0	0	0	0	0	0	0	0	0	0	0	0	e = ps_8u_5ul
2	2	0	3	0	8	5	2	2	5	0	0	0	0	0	0	0	0	0	0	0	0	0	0	0	0	0	0	0	0	0	0	0	0	0	0	0	0	0	0	0	0	0	0	0	0	0	0	0	0	0	1	0	0	f = ps_8u_6ul
2	0	1	1	0	4	7	5	4	2	0	0	0	0	0	0	0	0	0	0	0	0	0	0	0	0	0	0	0	0	0	0	0	2	0	0	1	0	0	0	1	0	0	0	0	0	0	0	0	0	0	0	0	0	g = ps_8u_7ul
0	0	0	5	0	0	5	15	3	0	0	0	0	0	0	0	0	0	0	0	0	0	0	1	0	0	0	0	0	1	0	0	0	0	0	0	0	0	0	0	0	0	0	0	0	0	0	0	0	0	0	0	0	0	h = ps_8u_8ul
0	0	0	0	3	2	5	3	6	7	0	0	0	0	0	0	0	0	0	0	0	0	0	0	0	0	0	0	0	0	0	0	0	2	0	0	0	0	0	0	0	0	0	0	0	0	0	0	1	1	0	0	0	0	i = ps_8u_9ul
0	0	0	0	0	5	0	2	2	21	0	0	0	0	0	0	0	0	0	0	0	0	0	0	0	0	0	0	0	0	0	0	0	0	0	0	0	0	0	0	0	0	0	0	0	0	0	0	0	0	0	0	0	0	j = ps_8u_10ul
0	0	0	0	0	0	0	0	0	0	26	1	0	1	1	1	0	0	0	0	0	0	0	0	0	0	0	0	0	0	0	0	0	0	0	0	0	0	0	0	0	0	0	0	0	0	0	0	0	0	0	0	0	0	k = ps_10u_1ul
0	0	0	0	0	0	0	0	0	0	5	23	0	0	1	0	0	1	0	0	0	0	0	0	0	0	0	0	0	0	0	0	0	0	0	0	0	0	0	0	0	0	0	0	0	0	0	0	0	0	0	0	0	0	l = ps_10u_2ul
0	0	0	0	0	0	0	0	0	0	0	0	30	0	0	0	0	0	0	0	0	0	0	0	0	0	0	0	0	0	0	0	0	0	0	0	0	0	0	0	0	0	0	0	0	0	0	0	0	0	0	0	0	0	m = ps_10u_3ul
0	0	1	0	0	0	0	0	0	0	5	0	0	16	2	3	0	0	2	0	1	0	0	0	0	0	0	0	0	0	0	0	0	0	0	0	0	0	0	0	0	0	0	0	0	0	0	0	0	0	0	0	0	0	n = ps_10u_4ul
0	0	0	0	0	0	0	0	0	0	2	2	0	1	18	4	1	1	0	0	1	0	0	0	0	0	0	0	0	0	0	0	0	0	0	0	0	0	0	0	0	0	0	0	0	0	0	0	0	0	0	0	0	0	o = ps_10u_5ul
0	0	0	0	0	0	0	0	0	0	0	0	0	2	5	16	4	1	0	1	0	0	0	1	0	0	0	0	0	0	0	0	0	0	0	0	0	0	0	0	0	0	0	0	0	0	0	0	0	0	0	0	0	0	p = ps_10u_6ul
0	0	0	0	0	0	0	0	0	0	0	0	0	2	1	5	17	1	3	0	0	0	0	0	0	1	0	0	0	0	0	0	0	0	0	0	0	0	0	0	0	0	0	0	0	0	0	0	0	0	0	0	0	0	q = ps_10u_7ul
0	0	0	0	0	0	0	0	0	0	0	1	0	0	0	1	2	20	6	0	0	0	0	0	0	0	0	0	0	0	0	0	0	0	0	0	0	0	0	0	0	0	0	0	0	0	0	0	0	0	0	0	0	0	r = ps_10u_8ul
0	0	0	0	0	0	0	0	0	0	0	1	0	0	1	0	4	4	16	1	0	0	1	1	1	0	0	0	0	0	0	0	0	0	0	0	0	0	0	0	0	0	0	0	0	0	0	0	0	0	0	0	0	0	s = ps_10u_9ul
0	0	0	0	0	0	0	0	0	0	0	0	0	0	0	0	0	0	0	30	0	0	0	0	0	0	0	0	0	0	0	0	0	0	0	0	0	0	0	0	0	0	0	0	0	0	0	0	0	0	0	0	0	0	t = ps_10u_10ul
0	0	0	1	0	2	0	0	0	0	2	0	0	1	0	1	0	0	0	0	7	0	1	2	4	1	0	2	2	1	0	0	0	0	0	0	0	1	0	0	0	0	0	1	0	0	0	0	0	0	0	1	0	0	u = me_1ul
0	0	0	2	3	1	0	0	0	0	0	1	2	1	0	0	0	0	0	1	3	3	2	2	1	0	0	2	3	1	0	0	0	0	0	0	0	1	0	0	0	0	0	0	0	0	0	0	0	1	0	0	0	0	v = me_2ul
0	0	0	1	0	0	0	1	0	0	0	0	0	0	0	0	0	0	3	0	6	1	6	5	2	0	0	0	0	3	0	0	0	1	0	0	0	0	0	0	0	0	0	0	0	0	0	0	0	0	0	0	1	0	w = me_3ul
0	0	0	0	1	0	1	0	0	0	0	0	2	0	0	0	1	0	0	1	3	4	3	7	1	3	1	0	0	0	0	0	0	1	0	0	0	0	1	0	0	0	0	0	0	0	0	0	0	0	0	0	0	0	x = me_4ul
0	0	0	0	0	0	0	0	0	0	0	1	0	0	0	0	0	1	1	0	2	4	2	4	2	3	5	1	2	0	0	0	0	0	0	0	0	0	0	0	0	0	0	0	0	0	0	0	0	0	0	2	0	0	y = me_5ul
0	0	0	0	0	0	0	0	0	0	0	1	1	0	0	0	0	1	1	2	2	1	1	5	2	8	3	1	0	1	0	0	0	0	0	0	0	0	0	0	0	0	0	0	0	0	0	0	0	0	0	0	0	0	z = me_6ul
0	0	0	0	1	0	0	0	0	0	0	0	0	0	0	0	0	1	1	1	0	3	2	0	2	5	4	4	4	1	0	0	0	0	0	0	0	0	1	0	0	0	0	0	0	0	0	0	0	0	0	0	0	0	aa = me_7ul
0	0	0	0	0	1	0	0	0	0	0	0	0	0	0	0	0	0	0	0	3	1	1	0	3	6	5	5	3	2	0	0	0	0	0	0	0	0	0	0	0	0	0	0	0	0	0	0	0	0	0	0	0	0	ab = me_8ul
0	0	0	0	0	0	0	0	0	0	0	1	0	0	0	0	0	0	0	0	0	0	1	1	1	1	4	5	3	11	0	0	0	0	0	0	0	1	0	0	0	1	0	0	0	0	0	0	0	0	0	0	0	0	ac = me_9ul
0	0	0	0	0	0	0	0	0	0	0	0	0	0	0	0	0	0	0	0	1	3	2	0	0	1	5	2	6	9	0	0	0	0	0	0	0	1	0	0	0	0	0	0	0	0	0	0	0	0	0	0	0	0	ad = me_10ul
0	0	1	0	0	0	0	0	0	0	0	0	0	0	0	0	0	0	0	0	0	0	0	0	0	0	0	0	0	0	20	2	3	0	0	0	0	0	0	0	0	0	0	0	1	0	0	0	1	0	1	1	0	0	ae = 25ppm_as
0	0	0	0	0	0	0	0	0	0	0	0	0	0	0	0	0	0	0	0	0	0	0	0	0	0	0	0	0	0	2	20	2	0	0	0	1	1	0	0	0	0	0	0	0	0	0	0	0	2	0	1	1	0	af = 50ppm_as
0	0	0	0	0	0	0	0	0	0	0	0	0	0	0	0	0	0	0	0	0	0	0	0	0	0	0	0	0	0	3	1	13	0	1	1	2	0	0	2	0	0	0	0	0	0	1	1	0	2	3	0	0	0	ag = 100ppm_as
1	0	0	0	0	0	1	0	3	0	0	0	0	0	0	0	0	0	0	0	0	0	0	0	0	0	0	0	0	0	0	0	1	15	5	0	0	0	0	0	0	0	0	0	3	0	0	0	0	0	0	0	1	0	ah = 25ppm_cd
1	0	0	0	0	1	0	0	0	1	0	0	0	0	0	0	0	0	0	0	0	0	0	0	0	0	0	0	0	0	0	3	4	4	12	0	1	0	0	0	0	0	0	0	2	0	0	0	0	0	1	0	0	0	ai = 50ppm_cd
1	0	1	0	0	0	0	0	0	0	0	0	0	0	0	0	0	0	0	0	0	0	0	0	0	0	0	0	0	0	0	0	0	0	0	18	0	0	0	0	0	0	0	0	1	1	2	0	3	2	1	0	0	0	aj = 100ppm_cd
0	0	0	0	0	0	0	0	0	0	0	0	0	0	0	0	0	0	0	0	0	0	0	0	0	0	0	0	0	0	1	3	0	0	2	1	13	4	1	0	0	0	2	0	0	0	0	0	0	0	2	0	0	1	ak = 25ppm_cr
0	0	0	0	0	0	0	0	0	0	0	0	0	0	0	0	0	0	0	0	0	0	0	0	0	0	0	0	0	0	0	1	0	0	0	0	0	26	2	0	0	0	0	0	0	0	0	0	0	0	0	0	1	0	al = 50ppm_cr
0	0	0	0	1	0	0	0	0	0	0	0	0	0	0	0	0	0	0	0	0	0	0	1	0	0	0	0	0	0	0	0	0	0	0	0	1	0	27	0	0	0	0	0	0	0	0	0	0	0	0	0	0	0	am = 100ppm_cr
0	0	0	0	0	0	0	0	0	0	0	0	0	0	0	0	0	0	0	0	0	0	0	1	0	0	0	0	0	0	0	2	0	0	0	0	0	0	0	12	6	4	0	0	0	0	0	0	0	0	0	0	3	2	an = 25ppm_cu
0	0	0	0	0	0	0	0	0	0	0	0	0	0	0	0	0	0	0	0	0	0	1	0	0	0	0	0	0	0	2	0	0	0	0	0	0	0	0	4	14	6	0	0	0	0	0	0	0	0	0	0	2	1	ao = 50ppm_cu
0	0	0	0	0	0	0	0	0	0	0	0	0	0	0	0	0	0	0	0	0	0	0	0	0	0	0	0	0	0	0	0	0	0	0	0	0	1	0	1	10	18	0	0	0	0	0	0	0	0	0	0	0	0	ap = 100ppm_cu
0	2	0	0	0	0	0	0	0	0	0	0	0	0	0	0	0	0	0	0	0	0	0	0	0	0	0	0	0	0	1	0	0	0	0	0	0	0	1	0	0	0	23	1	0	0	1	1	0	0	0	0	0	0	aq = 25ppm_hg
1	2	0	1	0	0	0	0	1	0	0	0	0	0	0	0	0	0	0	0	0	0	0	1	0	0	0	0	0	0	0	0	0	0	0	1	0	0	1	0	0	0	4	11	3	1	1	1	1	0	0	0	0	0	ar = 50ppm_hg
1	0	1	0	0	0	0	0	0	0	0	0	0	0	0	0	0	0	0	0	0	1	0	0	0	0	0	0	0	0	3	1	1	3	2	0	1	0	0	0	0	0	0	1	9	0	1	1	3	1	0	0	0	0	as = 100ppm_hg
0	0	0	0	0	0	0	0	0	0	0	0	0	0	0	0	0	0	0	0	0	0	0	0	0	0	0	0	0	0	0	0	2	1	0	2	0	0	0	0	0	0	2	0	0	22	1	0	0	0	0	0	0	0	at = 25ppm_ni
1	1	0	0	0	0	0	0	0	0	0	0	0	0	0	0	0	0	0	0	0	0	0	0	0	0	0	0	0	0	1	0	2	0	0	0	1	0	1	0	0	0	1	0	0	2	12	6	0	1	1	0	0	0	au = 50ppm_ni
0	0	0	0	0	0	1	0	0	0	0	0	0	0	0	0	0	0	0	0	0	0	0	0	0	0	0	1	0	0	2	1	2	0	0	0	0	0	0	0	0	0	2	1	2	0	3	12	0	3	0	0	0	0	av = 100ppm_ni
0	0	0	0	0	0	0	0	0	0	0	0	0	0	0	0	0	0	0	0	0	0	0	0	0	0	0	0	0	0	2	0	1	0	0	1	0	0	0	0	0	0	4	1	0	0	0	0	18	3	0	0	0	0	aw = 25ppm_pb
0	0	0	0	0	0	0	0	0	0	0	0	0	0	0	0	0	0	0	0	0	0	0	0	0	0	0	0	0	1	1	0	3	1	0	6	1	0	0	1	0	0	0	0	0	0	2	2	2	7	3	0	0	0	ax = 50ppm_pb
0	0	0	0	0	0	0	0	0	0	0	0	0	0	0	0	0	0	0	0	0	0	0	0	0	0	0	0	0	0	1	0	3	4	0	3	2	0	0	0	0	0	0	0	0	0	2	0	0	2	11	0	0	2	ay = 100ppm_pb
0	0	0	0	0	0	0	0	0	0	0	0	0	0	0	0	0	0	0	0	0	0	0	0	0	0	0	0	0	0	0	0	0	0	0	2	0	0	0	1	1	0	0	0	0	0	0	0	0	0	0	20	5	1	az = 25ppm_zn
0	0	0	0	0	0	0	0	0	0	0	0	0	0	0	0	0	0	0	0	0	0	0	0	0	0	0	0	0	0	0	0	0	0	0	0	0	0	0	6	0	0	0	0	0	0	0	0	0	0	0	3	16	5	ba = 50ppm_zn
0	0	0	0	0	0	0	0	0	0	0	0	0	0	0	0	0	0	0	0	0	0	0	0	0	0	0	0	0	0	0	0	0	0	0	0	0	0	0	3	0	0	0	0	0	0	0	0	0	0	0	0	7	20	bb = 100ppm_zn

Fig. 5. Confusion matrix of concentration-dependent classification results for combined data using 10-fold cross validation.

a	b	c	d	e	f	g	h	i	j	k	l	m	n	o	p	q	r	s	t	u	v	w	x	y	z	aa	ab	ac	ad	ae	af	ag	ah	ai	aj	ak	al	am	an	ao	ap	aq	ar	as	at	au	av	aw	ax	ay	az	ba	bb	<-- classified as
5	0	0	0	0	1	0	0	0	0	0	0	0	0	0	0	0	0	0	0	0	0	0	0	0	0	0	0	0	0	1	0	1	0	1	0	0	0	0	0	0	0	0	0	1	0	0	0	0	0	0	0	0	0	a = ps_8u_1ul
1	3	1	2	2	0	0	0	0	0	0	0	0	0	1	0	0	0	0	0	1	0	0	0	0	0	0	0	0	0	0	0	0	0	0	0	0	0	0	0	0	0	0	2	0	0	0	0	0	0	0	0	0	0	b = ps_8u_2ul
0	2	4	1	1	0	0	0	0	0	0	0	0	1	0	0	0	0	0	0	0	0	0	0	1	0	0	0	0	0	0	0	0	0	0	1	0	0	0	0	0	0	0	0	0	0	0	0	0	0	0	0	0	0	c = ps_8u_3ul
0	0	2	4	1	0	0	0	1	0	0	0	0	0	1	0	0	0	0	0	0	0	0	1	0	0	0	0	0	0	0	0	0	0	0	0	0	0	0	0	0	0	0	0	0	0	0	0	0	0	0	0	0	0	d = ps_8u_4ul
0	2	0	2	5	0	0	0	1	0	0	0	0	0	0	0	0	0	0	0	0	0	0	0	0	0	0	0	0	0	0	0	0	0	0	0	0	0	0	0	0	0	0	1	0	0	0	0	0	0	0	0	0	0	e = ps_8u_5ul
1	2	0	1	0	4	0	0	1	1	0	0	0	0	0	0	0	0	0	0	0	0	0	0	0	0	0	1	0	0	0	0	0	0	0	0	0	0	0	0	0	0	0	0	0	0	0	0	0	0	0	0	0	0	f = ps_8u_6ul
1	0	0	0	1	2	3	1	2	3	0	0	0	0	0	0	0	0	0	0	0	0	0	0	0	0	0	0	0	0	0	0	0	0	0	0	0	0	0	0	0	0	0	0	0	0	0	0	0	0	0	0	0	0	g = ps_8u_7ul
0	0	0	2	2	0	2	5	0	1	0	0	0	0	0	0	0	0	0	0	0	0	0	1	0	0	0	0	0	0	0	0	0	0	0	0	0	0	0	0	0	0	0	0	0	0	0	0	0	0	0	0	0	0	h = ps_8u_8ul
0	0	0	0	0	1	1	0	1	3	0	0	0	0	0	0	0	0	0	0	0	0	0	1	0	0	0	0	0	0	0	0	0	3	0	0	0	0	0	0	0	0	0	0	0	0	0	1	0	0	0	0	0	0	i = ps_8u_9ul
0	0	0	0	0	1	0	0	2	5	0	0	0	0	0	0	0	0	0	0	0	0	0	0	0	0	0	0	0	1	0	0	1	0	0	0	0	0	0	0	0	0	0	0	0	0	0	0	0	0	0	0	0	0	j = ps_8u_10ul
0	0	0	0	0	0	0	0	0	0	8	0	0	2	2	0	0	0	1	0	0	1	0	0	0	0	0	0	0	0	0	0	0	0	0	0	0	0	0	0	0	0	0	0	0	0	0	0	0	0	0	0	0	0	k = ps_10u_1ul
0	0	0	0	0	0	0	0	0	0	1	8	1	0	0	0	0	0	0	0	0	0	0	0	0	0	0	0	0	0	0	0	0	0	0	0	0	0	0	0	0	0	0	0	0	0	0	0	0	0	0	0	0	0	l = ps_10u_2ul
0	0	0	0	0	0	0	0	0	0	0	0	10	0	0	0	0	0	0	0	0	0	0	0	0	0	0	0	0	0	0	0	0	0	0	0	0	0	0	0	0	0	0	0	0	0	0	0	0	0	0	0	0	0	m = ps_10u_3ul
0	0	0	0	0	0	0	0	0	0	0	0	0	7	1	1	0	0	2	0	1	0	0	0	0	0	0	0	0	0	0	0	0	0	0	0	0	0	0	0	0	0	0	0	0	0	0	0	0	0	0	0	0	0	n = ps_10u_4ul
0	0	0	0	0	0	0	0	0	0	3	5	0	1	1	2	0	1	0	0	0	0	0	0	0	0	0	0	0	0	0	0	0	0	0	0	0	0	0	0	0	0	0	0	0	0	0	0	0	0	0	0	0	0	o = ps_10u_5ul
0	0	0	0	0	0	0	0	0	0	0	0	0	0	1	5	4	0	0	0	0	0	0	0	0	0	0	0	0	0	0	0	0	0	0	0	0	0	0	0	0	0	0	0	0	0	0	0	0	0	0	0	0	0	p = ps_10u_6ul
0	0	0	0	0	0	0	0	0	0	0	0	0	3	0	4	3	0	0	0	0	0	0	0	0	0	0	0	0	0	0	0	0	0	0	0	0	0	0	0	0	0	0	0	0	0	0	0	0	0	0	0	0	0	q = ps_10u_7ul
0	0	0	0	0	0	0	0	0	0	0	0	0	0	0	0	2	3	2	0	1	1	0	0	0	0	0	0	0	0	0	0	0	0	0	0	0	0	0	0	0	0	0	0	0	0	0	0	0	0	0	0	0	0	r = ps_10u_8ul
0	0	0	0	0	0	0	0	0	0	0	0	0	0	0	0	0	0	6	0	0	0	0	0	0	0	0	0	0	0	0	0	0	0	0	0	0	0	0	0	0	0	0	0	0	0	0	0	0	0	0	0	0	0	s = ps_10u_9ul
0	0	0	0	0	0	0	0	0	0	0	0	0	0	0	0	0	0	0	9	0	0	0	0	0	0	0	0	0	0	0	0	0	0	0	0	0	0	0	0	0	0	0	0	0	0	0	0	0	0	0	0	0	0	t = ps_10u_10ul
0	0	0	0	0	0	0	0	0	0	0	0	0	0	0	1	0	0	0	0	5	0	1	0	1	0	0	1	1	0	0	0	0	0	0	0	0	0	0	0	0	0	0	0	0	0	0	0	0	0	0	0	0	0	u = me_1ul
0	0	0	0	2	1	0	0	0	0	0	1	0	0	0	0	1	0	0	0	1	0	0	0	1	0	0	0	3	0	0	0	0	0	0	0	0	0	0	0	0	0	0	0	0	0	0	0	0	0	0	0	0	0	v = me_2ul
0	0	0	0	0	0	0	0	0	0	0	0	0	0	0	1	0	0	0	0	2	0	2	2	1	1	0	1	1	0	0	0	1	0	0	0	0	0	0	0	0	0	0	0	0	0	0	1	0	0	0	0	0	0	w = me_3ul
0	0	0	0	0	0	0	0	0	0	0	0	0	0	0	0	0	0	0	0	1	2	0	0	2	2	0	0	0	0	0	0	0	0	0	0	0	0	0	0	0	0	0	0	0	0	0	0	0	0	0	0	0	0	x = me_4ul
0	0	0	0	0	0	0	0	0	0	0	0	0	0	0	0	0	0	0	0	0	1	0	1	2	0	1	0	2	1	0	0	0	0	0	0	0	0	0	0	0	0	0	0	0	0	0	0	0	0	0	0	0	0	y = me_5ul
0	0	0	0	0	0	0	0	0	0	0	0	0	0	0	0	0	0	1	2	1	1	0	1	0	2	2	2	0	0	0	0	0	0	0	0	0	0	0	0	0	0	0	0	0	0	0	0	0	0	0	0	0	0	z = me_6ul
0	0	0	0	1	0	0	0	0	0	0	0	0	0	0	0	0	0	0	0	0	0	0	0	1	2	1	1	1	1	0	0	0	0	0	0	0	0	0	0	0	0	0	0	0	0	0	0	0	0	0	0	0	0	aa = me_7ul
0	0	0	0	1	0	0	0	0	0	0	0	0	0	0	0	0	0	0	0	0	0	0	2	0	3	1	1	0	0	0	0	0	0	0	0	0	0	0	0	0	0	0	0	0	0	0	0	0	0	0	0	0	0	ab = me_8ul
0	0	0	0	0	0	0	0	0	1	0	0	0	0	0	0	0	0	0	0	1	0	0	0	0	0	0	0	2	4	0	0	0	0	0	0	0	0	0	0	0	0	0	0	0	0	0	0	0	0	0	0	0	0	ac = me_9ul
0	0	0	0	0	0	0	0	0	0	0	0	0	0	0	0	1	0	0	0	1	0	1	0	0	0	1	1	6	3	0	0	0	0	0	0	0	1	0	0	0	0	0	0	0	0	0	0	0	0	0	0	0	0	ad = me_10ul
0	0	0	0	0	0	0	0	0	0	0	0	0	0	0	0	0	0	0	0	0	0	0	0	0	0	0	0	0	0	2	1	0	0	0	0	1	0	0	0	0	0	0	1	0	0	0	0	0	3	0	0	0	0	ae = 25ppm_as
0	0	0	0	0	0	0	0	0	0	0	0	0	0	0	0	0	0	0	0	0	0	0	0	0	0	0	0	0	0	0	8	0	0	0	0	2	0	0	0	0	0	0	0	0	0	0	0	0	0	1	0	0	0	af = 50ppm_as
0	0	0	0	0	0	0	0	0	0	0	0	0	0	0	0	0	0	0	0	0	0	0	0	0	0	0	0	0	0	0	1	2	0	0	0	2	0	0	1	0	0	0	0	0	0	0	0	0	0	3	0	0	0	ag = 100ppm_as
0	0	0	0	0	1	0	0	0	0	0	0	0	0	0	0	0	0	0	0	0	0	0	0	0	0	0	0	0	0	0	0	0	4	1	1	0	0	0	0	0	0	0	0	0	0	0	0	0	0	2	0	0	0	ah = 25ppm_cd
0	0	0	0	0	0	1	0	0	0	0	0	0	1	0	0	0	0	0	0	0	0	0	0	0	0	0	0	0	0	1	1	0	2	3	0	0	0	0	0	0	0	0	0	0	1	0	0	0	0	0	0	0	0	ai = 50ppm_cd
0	0	0	0	0	0	0	0	0	0	0	0	0	0	0	0	0	0	0	0	0	0	0	0	0	0	0	0	0	0	0	0	0	0	0	7	0	0	0	0	0	0	0	0	2	1	0	0	1	0	0	0	0	0	aj = 100ppm_cd
0	0	0	0	0	0	0	0	0	0	0	0	0	0	0	0	0	0	0	0	0	0	0	0	0	0	0	0	0	0	1	1	0	1	1	5	2	0	0	0	0	0	0	0	0	1	0	0	0	0	0	0	0	0	ak = 25ppm_cr
0	0	0	0	0	0	0	0	0	0	0	0	0	0	0	0	0	0	0	0	0	0	0	0	0	0	0	0	1	0	0	0	0	0	0	0	0	7	0	0	0	0	0	0	0	0	0	0	0	0	0	0	0	0	al = 50ppm_cr
0	0	0	0	0	0	0	0	0	0	0	0	0	0	0	0	0	0	0	0	0	0	0	0	1	0	0	0	0	0	0	0	0	0	0	0	2	0	5	0	0	0	0	0	0	0	0	0	0	0	0	0	0	0	am = 100ppm_cr
0	0	0	0	0	0	0	0	0	0	0	0	0	0	0	0	0	0	0	0	0	0	0	0	0	0	0	0	0	0	0	0	0	0	0	0	0	0	0	3	2	0	0	0	0	0	0	0	0	0	0	0	1	1	an = 25ppm_cu
0	0	0	0	0	0	0	0	0	0	0	0	0	0	0	0	0	0	0	0	0	0	0	0	0	0	0	0	0	0	0	0	0	0	0	0	0	0	0	0	4	3	0	0	0	0	0	0	0	1	0	0	2	2	ao = 50ppm_cu
0	0	0	0	0	0	0	0	0	0	0	0	0	0	0	0	0	0	0	0	0	0	0	0	0	0	0	0	0	0	0	0	0	0	0	0	0	0	0	0	1	6	0	0	0	0	0	0	0	0	0	0	0	0	ap = 100ppm_cu
0	0	0	0	0	0	0	0	0	0	0	0	0	0	0	0	0	0	0	0	0	0	0	0	0	0	0	0	0	0	2	0	0	0	0	0	0	0	0	0	0	0	10	0	0	0	0	0	0	0	0	0	0	0	aq = 25ppm_hg
0	0	0	1	1	0	0	0	0	0	0	0	0	0	0	0	0	0	0	0	0	0	0	0	0	0	0	0	0	0	0	0	0	0	0	0	0	0	0	0	0	0	1	3	0	1	0	1	0	0	0	0	0	0	ar = 50ppm_hg
1	0	0	0	0	0	0	0	0	0	0	0	0	0	0	0	0	0	0	0	0	0	0	0	0	0	0	0	0	0	1	1	2	0	1	0	0	0	0	0	0	0	0	1	1	0	0	0	0	2	0	0	0	0	as = 100ppm_hg
1	0	0	0	0	0	0	0	0	0	0	0	0	0	0	0	0	0	0	0	0	0	0	0	0	0	0	0	0	0	0	0	1	0	0	0	0	0	0	0	0	0	0	1	0	7	0	0	0	0	0	0	0	0	at = 25ppm_ni
0	0	0	0	0	0	0	0	0	0	0	0	0	0	0	0	0	0	0	0	0	0	0	0	0	0	0	0	0	0	0	0	1	0	0	0	0	0	0	0	0	0	0	1	0	0	6	0	0	0	0	0	0	0	au = 50ppm_ni
0	0	0	0	0	0	2	0	0	0	0	0	0	0	0	0	0	0	0	0	0	0	0	0	0	0	0	0	0	0	0	0	0	0	1	0	0	0	0	0	0	0	0	1	0	0	1	5	0	0	0	0	0	0	av = 100ppm_ni
0	0	0	0	0	0	0	0	0	0	0	0	0	0	0	0	0	0	0	0	0	0	0	0	0	0	0	0	0	0	1	0	0	0	0	0	0	0	0	0	0	0	0	0	4	0	0	0	7	0	0	1	0	0	aw = 25ppm_pb
0	0	0	0	0	0	0	0	0	0	0	0	0	0	0	0	0	0	0	0	0	0	0	0	0	0	0	0	0	0	0	0	0	0	0	1	0	0	0	1	0	0	0	0	0	3	2	0	3	1	0	0	0	0	ax = 50ppm_pb
0	0	0	0	0	0	0	0	0	0	0	0	0	0	0	0	0	0	0	0	0	0	0	0	0	0	0	0	0	0	1	0	0	0	1	0	1	0	0	0	0	0	0	0	0	0	0	0	0	0	4	0	0	0	ay = 100ppm_pb
0	0	0	0	0	0	0	0	0	0	0	0	0	0	0	0	0	0	0	0	0	0	0	0	0	0	0	0	0	0	0	0	0	0	0	0	0	0	0	0	0	0	0	0	0	0	0	0	0	1	0	6	0	0	az = 25ppm_zn
0	0	0	0	0	0	0	0	0	0	0	0	0	0	0	0	0	0	0	0	0	0	0	0	0	0	0	0	0	0	0	0	0	0	0	0	0	0	0	0	0	0	0	0	0	0	0	0	0	0	0	3	5	3	ba = 50ppm_zn
0	0	0	0	0	0	0	0	0	0	0	0	0	0	0	0	0	0	0	0	0	0	0	0	0	0	0	0	0	0	0	0	0	0	0	0	0	0	0	0	0	0	0	0	0	0	0	0	0	0	0	0	1	5	bb = 100ppm_zn

Fig. 6. Confusion matrix of concentration-dependent classification results for combined data using 66 % training and 33 % test data.

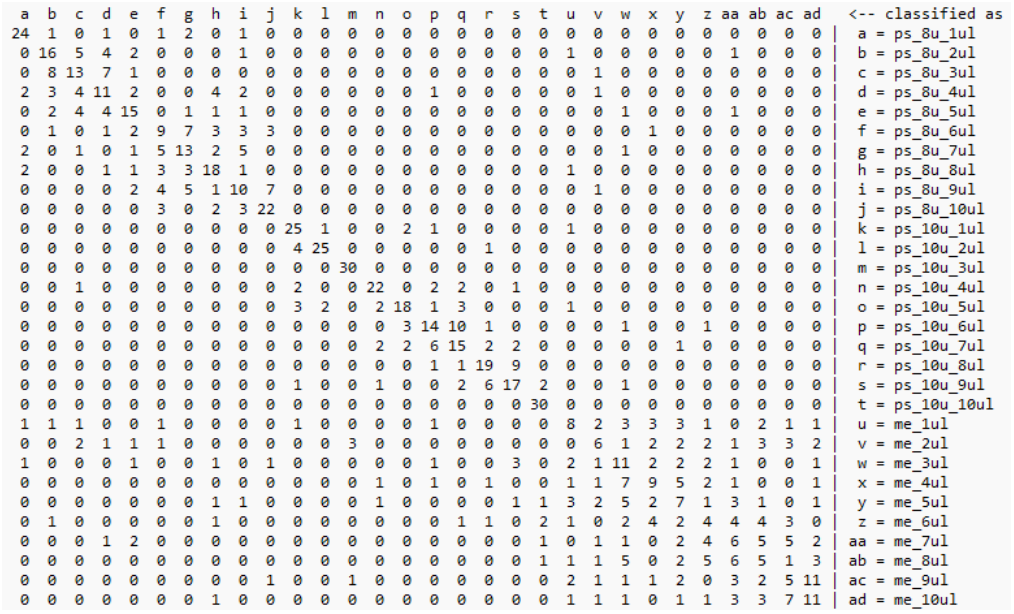

a	b	c	d	e	f	g	h	i	j	k	l	m	n	o	p	q	r	s	t	u	v	w	x	y	z	aa	ab	ac	ad	<-- classified as
24	1	0	1	0	1	2	0	1	0	0	0	0	0	0	0	0	0	0	0	0	0	0	0	0	0	0	0	0	0	a = ps_8u_1ul
0	16	5	4	2	0	0	0	1	0	0	0	0	0	0	0	0	0	0	0	1	0	0	0	0	0	1	0	0	0	b = ps_8u_2ul
0	8	13	7	1	0	0	0	0	0	0	0	0	0	0	0	0	0	0	0	1	0	0	0	0	0	0	0	0	0	c = ps_8u_3ul
2	3	4	11	2	0	0	4	2	0	0	0	0	0	0	1	0	0	0	0	0	1	0	0	0	0	0	0	0	0	d = ps_8u_4ul
0	2	4	4	15	0	1	1	1	0	0	0	0	0	0	0	0	0	0	0	0	0	1	0	0	0	1	0	0	0	e = ps_8u_5ul
0	1	0	1	2	9	7	3	3	3	0	0	0	0	0	0	0	0	0	0	0	0	1	0	0	0	0	0	0	0	f = ps_8u_6ul
2	0	1	0	1	5	13	2	5	0	0	0	0	0	0	0	0	0	0	0	0	0	1	0	0	0	0	0	0	0	g = ps_8u_7ul
2	0	0	1	1	3	3	18	1	0	0	0	0	0	0	0	0	0	0	0	1	0	0	0	0	0	0	0	0	0	h = ps_8u_8ul
0	0	0	0	2	4	5	1	10	7	0	0	0	0	0	0	0	0	0	0	1	0	0	0	0	0	0	0	0	0	i = ps_8u_9ul
0	0	0	0	0	3	0	2	3	22	0	0	0	0	0	0	0	0	0	0	0	0	0	0	0	0	0	0	0	0	j = ps_8u_10ul
0	0	0	0	0	0	0	0	0	0	25	1	0	0	2	1	0	0	0	0	1	0	0	0	0	0	0	0	0	0	k = ps_10u_1ul
0	0	0	0	0	0	0	0	0	0	4	25	0	0	0	0	0	1	0	0	0	0	0	0	0	0	0	0	0	0	l = ps_10u_2ul
0	0	0	0	0	0	0	0	0	0	0	0	30	0	0	0	0	0	0	0	0	0	0	0	0	0	0	0	0	0	m = ps_10u_3ul
0	0	1	0	0	0	0	0	0	0	2	0	0	22	0	2	2	0	1	0	0	0	0	0	0	0	0	0	0	0	n = ps_10u_4ul
0	0	0	0	0	0	0	0	0	0	3	2	0	2	18	1	3	0	0	0	1	0	0	0	0	0	0	0	0	0	o = ps_10u_5ul
0	0	0	0	0	0	0	0	0	0	0	0	0	0	3	14	10	1	0	0	0	0	1	0	0	1	0	0	0	0	p = ps_10u_6ul
0	0	0	0	0	0	0	0	0	0	0	0	0	2	2	6	15	2	2	0	0	0	0	0	1	0	0	0	0	0	q = ps_10u_7ul
0	0	0	0	0	0	0	0	0	0	0	0	0	0	0	1	1	19	9	0	0	0	0	0	0	0	0	0	0	0	r = ps_10u_8ul
0	0	0	0	0	0	0	0	0	0	1	0	0	1	0	0	2	6	17	2	0	0	1	0	0	0	0	0	0	0	s = ps_10u_9ul
0	0	0	0	0	0	0	0	0	0	0	0	0	0	0	0	0	0	0	30	0	0	0	0	0	0	0	0	0	0	t = ps_10u_10ul
1	1	1	0	0	1	0	0	0	0	1	0	0	0	0	1	0	0	0	0	8	2	3	3	3	1	0	2	1	1	u = me_1ul
0	0	2	1	1	1	0	0	0	0	0	3	0	0	0	0	0	0	0	0	6	1	2	2	2	1	3	3	2		v = me_2ul
1	0	0	0	1	0	0	1	0	1	0	0	0	0	0	1	0	0	3	0	2	1	11	2	2	2	1	0	0	1	w = me_3ul
0	0	0	0	0	0	0	0	0	0	0	0	0	1	0	1	0	1	0	0	1	1	7	9	5	2	1	0	0	1	x = me_4ul
0	0	0	0	0	0	0	1	1	0	0	0	0	1	0	0	0	0	1	1	3	2	5	2	7	1	3	1	0	1	y = me_5ul
0	1	0	0	0	0	0	1	0	0	0	0	0	0	0	0	0	1	1	0	2	1	0	2	4	2	4	4	3	0	z = me_6ul
0	0	0	1	2	0	0	0	0	0	0	0	0	0	0	0	0	0	1	0	1	1	1	0	2	4	6	5	5	2	aa = me_7ul
0	0	0	0	0	0	0	0	0	0	0	0	0	0	0	0	0	0	0	0	1	1	1	5	0	2	5	6	5	1	3	ab = me_8ul
0	0	0	0	0	0	0	0	0	1	0	0	1	0	0	0	0	0	0	0	2	1	1	1	2	0	3	2	5	11	ac = me_9ul
0	0	0	0	0	0	0	1	0	0	0	0	0	0	0	0	0	0	0	0	1	1	1	0	1	1	3	3	7	11	ad = me_10ul

Fig. 7. Confusion matrix of concentration-dependent classification results for microplastics using 10-fold cross validation.

a	b	c	d	e	f	g	h	i	j	k	l	m	n	o	p	q	r	s	t	u	v	w	x	y	z	aa	ab	ac	ad	<-- classified as
8	0	0	1	0	0	1	0	0	0	0	0	0	0	0	0	0	0	0	0	0	0	0	0	0	0	0	0	0	0	a = ps_8u_1ul
0	5	1	2	1	0	0	0	0	0	0	0	0	0	0	0	0	0	0	0	0	1	0	0	0	0	0	0	0	0	b = ps_8u_2ul
0	2	7	3	0	0	0	0	0	0	0	0	0	0	0	0	0	0	0	0	0	0	0	0	0	0	0	0	0	0	c = ps_8u_3ul
0	1	0	3	0	0	0	1	0	0	0	0	0	0	0	0	0	0	0	0	0	0	0	0	0	0	0	0	0	0	d = ps_8u_4ul
0	0	1	1	4	0	0	0	0	1	0	0	0	0	0	0	0	0	0	0	0	0	0	0	0	0	0	0	0	0	e = ps_8u_5ul
1	0	0	1	0	2	4	0	3	3	0	0	0	0	0	0	0	0	0	0	0	0	0	0	0	0	0	0	0	0	f = ps_8u_6ul
0	0	0	0	0	2	4	2	2	1	0	0	0	0	0	0	0	0	0	0	0	0	0	0	0	0	0	0	0	0	g = ps_8u_7ul
0	0	0	0	0	0	1	6	0	0	0	0	0	0	0	0	0	0	0	0	1	0	0	0	0	0	0	0	0	0	h = ps_8u_8ul
0	0	0	0	1	1	1	1	2	3	0	0	0	0	0	0	0	0	0	0	0	0	0	0	0	0	0	0	0	0	i = ps_8u_9ul
0	0	0	0	0	1	0	2	1	6	0	0	0	0	0	0	0	0	0	0	0	0	0	0	0	0	0	0	0	0	j = ps_8u_10ul
0	0	0	0	0	0	0	0	0	0	5	0	0	0	0	1	0	0	0	0	0	0	0	0	0	0	0	0	0	0	k = ps_10u_1ul
0	0	0	0	0	0	0	0	0	0	1	9	1	0	1	0	0	0	0	0	0	0	0	0	0	0	0	0	0	0	l = ps_10u_2ul
0	0	0	0	0	0	0	0	0	0	0	0	13	0	0	0	0	0	0	0	0	0	0	0	0	0	0	0	0	0	m = ps_10u_3ul
0	0	1	0	0	0	0	0	0	0	0	1	0	5	3	0	1	0	0	0	0	0	0	0	0	0	0	0	0	0	n = ps_10u_4ul
0	0	0	0	0	0	0	0	0	0	1	0	0	0	6	0	1	1	0	0	0	0	0	0	0	0	0	0	0	0	o = ps_10u_5ul
0	0	0	0	0	0	0	0	0	0	0	0	0	0	0	3	5	0	1	0	0	0	0	2	0	0	0	0	0	0	p = ps_10u_6ul
0	0	0	0	0	0	0	0	0	0	0	0	0	1	0	0	5	0	1	0	0	0	0	1	0	0	0	0	0	0	q = ps_10u_7ul
0	0	0	0	0	0	0	0	0	0	0	0	0	0	0	0	0	6	2	0	0	0	0	0	0	0	0	0	0	0	r = ps_10u_8ul
0	0	0	0	0	0	0	0	0	0	1	0	0	0	0	1	2	2	0	0	0	0	0	1	1	0	0	0	0	0	s = ps_10u_9ul
0	0	0	0	0	0	0	0	0	0	1	0	0	0	0	0	0	0	12	0	0	0	0	0	0	0	0	0	0	0	t = ps_10u_10ul
1	1	0	0	0	0	0	0	0	0	0	0	0	0	0	1	0	0	0	0	1	1	0	0	0	0	2	1	0		u = me_1ul
0	0	0	0	1	0	0	0	0	0	0	0	3	0	0	0	1	0	0	0	0	1	3	1	0	0	0	0	2		v = me_2ul
1	0	0	0	0	0	0	0	0	0	0	0	0	0	0	0	0	0	0	0	0	0	4	0	0	0	0	1	0	2	w = me_3ul
0	0	0	0	0	0	0	1	0	0	0	0	0	0	0	0	0	0	0	0	1	0	5	3	0	0	0	0	0	0	x = me_4ul
0	0	0	0	0	0	0	0	0	0	0	0	0	0	0	0	0	0	0	0	0	0	2	3	1	0	2	2	2	0	y = me_5ul
0	0	0	0	0	0	0	0	0	0	0	0	0	0	0	0	0	0	0	1	0	1	2	2	0	2	5	1	0	0	z = me_6ul
0	0	0	0	0	0	0	0	0	0	0	0	0	0	0	0	0	0	0	0	0	0	1	1	0	1	4	2	0	0	aa = me_7ul
0	0	0	1	0	0	0	0	0	0	0	0	0	0	0	0	0	0	0	0	0	0	0	0	0	2	2	4	0	0	ab = me_8ul
0	0	0	0	0	0	0	0	0	0	0	1	0	0	0	1	0	0	0	1	1	0	0	0	1	1	0	4	3		ac = me_9ul
0	0	0	0	0	0	0	0	0	0	0	0	0	0	0	0	1	0	0	0	1	1	0	0	1	0	1	0	3	2	ad = me_10ul

Fig. 8. Confusion matrix of concentration-dependent classification results for microplastics using 66 % training and 33 % test data.

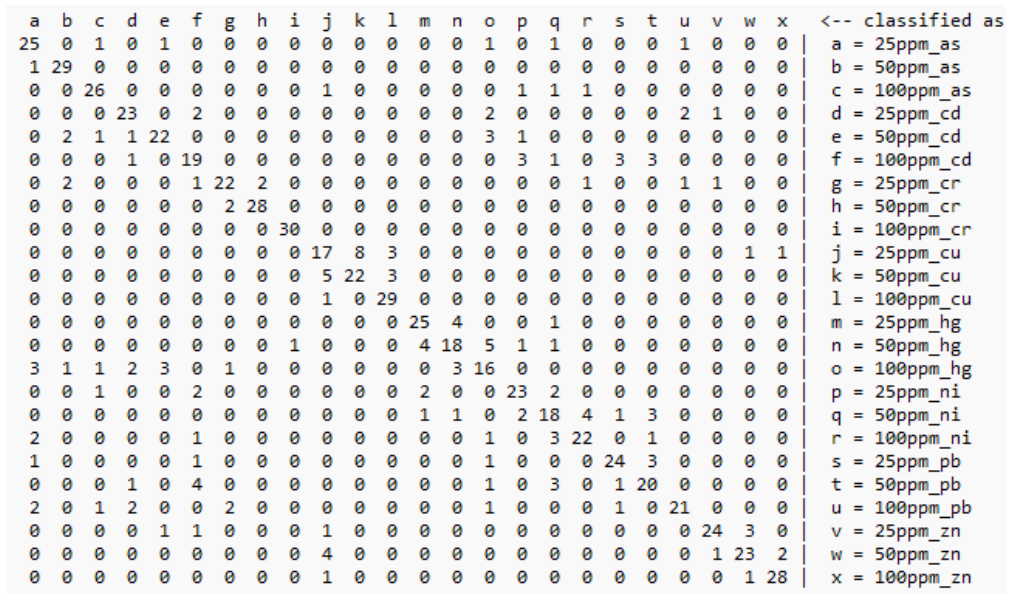

a	b	c	d	e	f	g	h	i	j	k	l	m	n	o	p	q	r	s	t	u	v	w	x	<-- classified as
25	0	1	0	1	0	0	0	0	0	0	0	0	0	1	0	1	0	0	0	1	0	0	0	a = 25ppm_as
1	29	0	0	0	0	0	0	0	0	0	0	0	0	0	0	0	0	0	0	0	0	0	0	b = 50ppm_as
0	0	26	0	0	0	0	0	0	1	0	0	0	0	0	1	1	1	0	0	0	0	0	0	c = 100ppm_as
0	0	0	23	0	2	0	0	0	0	0	0	0	0	0	2	0	0	0	0	0	2	1	0	d = 25ppm_cd
0	2	1	1	22	0	0	0	0	0	0	0	0	0	0	3	1	0	0	0	0	0	0	0	e = 50ppm_cd
0	0	0	1	0	19	0	0	0	0	0	0	0	0	0	3	1	0	3	3	0	0	0	0	f = 100ppm_cd
0	2	0	0	0	1	22	2	0	0	0	0	0	0	0	0	1	0	0	1	1	0	0	0	g = 25ppm_cr
0	0	0	0	0	0	2	28	0	0	0	0	0	0	0	0	0	0	0	0	0	0	0	0	h = 50ppm_cr
0	0	0	0	0	0	0	0	30	0	0	0	0	0	0	0	0	0	0	0	0	0	0	0	i = 100ppm_cr
0	0	0	0	0	0	0	0	0	17	8	3	0	0	0	0	0	0	0	0	0	0	1	1	j = 25ppm_cu
0	0	0	0	0	0	0	0	0	5	22	3	0	0	0	0	0	0	0	0	0	0	0	0	k = 50ppm_cu
0	0	0	0	0	0	0	0	0	1	0	29	0	0	0	0	0	0	0	0	0	0	0	0	l = 100ppm_cu
0	0	0	0	0	0	0	0	0	0	0	0	25	4	0	0	1	0	0	0	0	0	0	0	m = 25ppm_hg
0	0	0	0	0	0	0	0	0	1	0	0	0	4	18	5	1	1	0	0	0	0	0	0	n = 50ppm_hg
3	1	1	2	3	0	1	0	0	0	0	0	0	3	16	0	0	0	0	0	0	0	0	0	o = 100ppm_hg
0	0	1	0	0	2	0	0	0	0	0	0	2	0	0	23	2	0	0	0	0	0	0	0	p = 25ppm_ni
0	0	0	0	0	0	0	0	0	0	0	0	1	1	0	2	18	4	1	3	0	0	0	0	q = 50ppm_ni
2	0	0	0	0	1	0	0	0	0	0	0	0	0	1	0	3	22	0	1	0	0	0	0	r = 100ppm_ni
1	0	0	0	0	1	0	0	0	0	0	0	0	0	1	0	0	0	24	3	0	0	0	0	s = 25ppm_pb
0	0	0	1	0	4	0	0	0	0	0	0	0	0	1	0	3	0	1	20	0	0	0	0	t = 50ppm_pb
2	0	1	2	0	0	2	0	0	0	0	0	0	0	1	0	0	0	1	0	21	0	0	0	u = 100ppm_pb
0	0	0	0	1	1	0	0	0	1	0	0	0	0	0	0	0	0	0	0	0	24	3	0	v = 25ppm_zn
0	0	0	0	0	0	0	0	0	4	0	0	0	0	0	0	0	0	0	0	0	1	23	2	w = 50ppm_zn
0	0	0	0	0	0	0	0	0	1	0	0	0	0	0	0	0	0	0	0	0	0	1	28	x = 100ppm_zn

Fig. 9. Confusion matrix of concentration-dependent classification results for heavy metals using 10-fold cross validation.

a	b	c	d	e	f	g	h	i	j	k	l	m	n	o	p	q	r	s	t	u	v	w	x	<-- classified as
7	0	0	0	0	0	1	0	0	0	0	0	0	0	0	0	0	0	0	0	0	0	0	0	a = 25ppm_as
0	9	0	0	0	0	0	0	0	0	0	0	0	0	0	0	0	0	0	0	0	0	0	0	b = 50ppm_as
0	0	6	0	0	0	2	0	0	0	0	0	0	0	0	0	0	0	0	0	3	0	0	0	c = 100ppm_as
0	0	1	10	0	1	0	0	0	0	0	0	0	2	1	0	0	0	0	0	0	0	0	0	d = 25ppm_cd
0	1	1	0	4	0	0	0	0	0	1	0	0	0	0	0	0	1	1	0	0	0	1	0	e = 50ppm_cd
0	0	0	0	0	7	0	0	0	0	0	0	0	2	0	0	0	0	0	1	0	0	0	0	f = 100ppm_cd
1	0	0	0	1	0	3	1	0	0	0	0	0	0	0	0	0	0	0	1	0	0	0	0	g = 25ppm_cr
0	0	0	0	0	0	1	7	0	0	0	0	0	0	0	0	0	0	0	0	0	0	0	0	h = 50ppm_cr
0	0	0	0	0	0	0	0	13	0	0	0	0	0	0	0	0	0	0	0	0	0	0	0	i = 100ppm_cr
0	0	0	0	0	0	0	0	0	3	4	1	0	0	0	0	0	0	0	0	0	2	1		j = 25ppm_cu
0	1	0	0	0	0	0	0	0	2	5	2	0	0	0	0	0	0	0	0	0	0	0		k = 50ppm_cu
0	0	0	0	0	0	0	0	0	0	0	11	0	0	0	0	0	0	0	0	0	0	0		l = 100ppm_cu
0	0	0	0	0	0	0	0	0	0	0	0	9	1	0	0	0	3	0	0	0	0	0		m = 25ppm_hg
0	0	0	0	0	0	0	0	0	0	0	0	2	4	0	3	0	0	0	1	0	0	0		n = 50ppm_hg
0	1	0	0	1	0	0	0	0	0	0	0	0	4	3	0	0	0	0	0	0	0	0		o = 100ppm_hg
0	0	0	0	0	0	0	0	0	0	0	0	0	0	0	7	0	1	0	0	0	0	0		p = 25ppm_ni
0	0	2	0	0	0	0	0	0	0	0	0	2	1	0	1	5	1	1	2	0	0	0		q = 50ppm_ni
2	0	0	0	0	0	0	0	0	0	0	0	0	0	0	0	0	2	0	0	0	0	0		r = 100ppm_ni
0	0	0	0	0	0	0	0	0	0	0	0	0	0	1	0	0	0	5	2	0	0	0		s = 25ppm_pb
0	0	0	1	0	1	1	0	0	0	0	0	0	0	1	0	1	1	0	5	0	0	0		t = 50ppm_pb
0	0	0	0	1	0	2	0	0	0	0	0	0	0	1	0	0	0	1	0	4	0	0		u = 100ppm_pb
2	0	0	0	0	0	0	0	0	0	0	0	0	0	0	0	0	0	0	0	0	4	2		v = 25ppm_zn
0	0	0	0	0	0	0	0	0	2	0	0	0	0	0	0	0	0	0	0	0	0	10		w = 50ppm_zn
0	0	0	0	0	0	0	0	0	0	0	0	0	0	0	0	0	0	0	0	0	0	1	9	x = 100ppm_zn

Fig. 10. Confusion matrix of concentration-dependent classification results for heavy metals using 66 % training and 33 % test data.

a	b	c	d	e	f	g	h	i	j	k	<-- classified as
255	1	27	0	2	1	0	13	0	0	1	a = ps_8u
0	294	6	0	0	0	0	0	0	0	0	b = ps_10u
9	10	273	0	0	6	0	2	0	0	0	c = me_8u
3	2	3	14	2	13	6	13	15	8	11	d = as
16	0	9	2	16	5	1	14	6	10	11	e = cd
5	1	11	1	0	61	2	1	1	1	6	f = cr
0	0	0	0	0	0	77	0	0	0	13	g = cu
10	0	6	2	2	5	2	52	6	0	5	h = hg
5	1	9	1	1	7	1	18	36	4	7	i = ni
7	0	6	0	4	11	7	6	9	23	17	j = pb
1	0	1	1	0	1	17	0	0	2	67	k = zn

Fig. 11. Confusion matrix of concentration-independent classification results for combined data using 10-fold cross validation.

a	b	c	d	e	f	g	h	i	j	k	<-- classified as
111	0	1	0	0	0	0	1	0	0	0	a = ps_8u
0	99	4	0	0	0	0	0	0	0	0	b = ps_10u
3	5	91	0	0	0	0	0	0	0	0	c = me_8u
0	0	0	20	0	3	0	2	0	3	0	d = as
0	0	1	2	21	0	0	3	1	2	0	e = cd
1	0	0	0	0	25	0	0	0	2	0	f = cr
0	0	0	0	0	0	23	0	0	0	3	g = cu
3	0	0	0	1	1	0	22	3	0	0	h = hg
2	0	0	1	2	0	0	3	20	0	0	i = ni
0	0	0	1	1	1	0	1	7	19	1	j = pb
0	0	0	1	0	0	1	0	0	0	22	k = zn

Fig. 12. Confusion matrix of concentration-independent classification results for combined data using 66 % training and 33 % test data.

a	b	c	<-- classified as
295	0	5	a = ps_8u
0	292	8	b = ps_10u
8	6	286	c = me_8u

Fig. 13. Confusion matrix of concentration-independent classification results for microplastics using 10-fold cross validation.

a	b	c	<-- classified as
96	0	0	a = ps_8u
0	96	3	b = ps_10u
4	2	99	c = me_8u

Fig. 14. Confusion matrix of concentration-independent classification results for microplastics using 66 % training and 33 % test data.

a	b	c	d	e	f	g	h	<-- classified as
82	0	1	0	1	3	3	0	a = as
3	67	1	0	5	2	12	0	b = cd
2	1	87	0	0	0	0	0	c = cr
0	0	0	84	0	0	0	6	d = cu
4	4	1	0	77	3	1	0	e = hg
1	2	0	0	5	77	5	0	f = ni
8	13	0	0	1	5	63	0	g = pb
1	1	0	4	0	0	0	84	h = zn

Fig. 15. Confusion matrix of concentration-independent classification results for heavy metals using 10-fold cross validation.

a	b	c	d	e	f	g	h	<-- classified as
26	1	0	0	0	0	1	0	a = as
4	25	0	0	3	0	3	0	b = cd
1	1	26	0	0	0	0	0	c = cr
0	0	0	29	0	0	0	3	d = cu
0	1	0	0	26	5	0	0	e = hg
1	2	0	0	2	19	3	0	f = ni
0	5	2	0	1	2	18	0	g = pb
0	0	0	2	0	0	0	28	h = zn

Fig. 16. Confusion matrix of concentration-independent classification results for heavy metals using 66 % training and 33 % test data.

Fig. 17. Confusion matrix of concentration-dependent classification results for combined data using 10-fold cross validation with top 10 features selected.

Fig. 18. Confusion matrix of concentration-dependent classification results for combined data using 66 % training and 33 % test data with top 10 features selected.

a	b	c	d	e	f	g	h	i	j	k	l	m	n	o	p	q	r	s	t	u	v	w	x	y	z	aa	ab	ac	ad	<-- classified as
27	0	0	1	1	0	1	0	0	0	0	0	0	0	0	0	0	0	0	0	0	0	0	0	0	0	0	0	0	0	a = ps_8u_1ul
0	19	1	1	0	1	0	0	0	0	0	0	0	0	0	0	0	0	0	0	0	0	0	4	3	0	1	0	0	0	b = ps_8u_2ul
1	5	20	0	3	0	0	0	0	0	0	0	0	0	0	1	0	0	0	0	0	0	0	0	0	0	0	0	0	0	c = ps_8u_3ul
2	0	4	18	2	0	0	0	0	0	0	0	0	0	0	0	0	0	0	0	0	1	0	2	1	0	0	0	0	0	d = ps_8u_4ul
2	0	1	6	18	1	0	0	2	0	0	0	0	0	0	0	0	0	0	0	0	0	0	0	0	0	0	0	0	0	e = ps_8u_5ul
0	0	0	0	0	17	3	3	6	1	0	0	0	0	0	0	0	0	0	0	0	0	0	0	0	0	0	0	0	0	f = ps_8u_6ul
0	0	0	0	0	8	10	2	10	0	0	0	0	0	0	0	0	0	0	0	0	0	0	0	0	0	0	0	0	0	g = ps_8u_7ul
4	0	0	8	0	1	0	11	1	3	0	0	0	0	0	0	0	0	0	0	0	0	2	0	0	0	0	0	0	0	h = ps_8u_8ul
0	0	0	0	1	1	3	1	14	8	0	0	0	0	0	0	0	0	0	0	0	0	2	0	0	0	0	0	0	0	i = ps_8u_9ul
0	0	0	0	0	1	0	0	1	28	0	0	0	0	0	0	0	0	0	0	0	0	0	0	0	0	0	0	0	0	j = ps_8u_10ul
0	0	0	0	0	0	0	0	0	0	28	1	0	0	0	0	0	0	0	0	0	0	0	0	0	0	0	0	1	0	k = ps_10u_1ul
0	0	0	0	0	0	0	0	0	0	0	30	0	0	0	0	0	0	0	0	0	0	0	0	0	0	0	0	0	0	l = ps_10u_2ul
0	0	0	0	0	0	0	0	0	0	0	0	29	0	0	0	0	0	0	0	0	0	0	0	0	0	0	0	0	1	m = ps_10u_3ul
0	0	6	0	0	0	0	0	0	0	0	0	0	16	0	1	1	0	0	0	0	2	0	4	0	0	0	0	0	0	n = ps_10u_4ul
0	0	0	0	0	0	0	0	0	0	0	1	0	5	12	1	6	0	0	0	0	0	4	1	0	0	0	0	0	0	o = ps_10u_5ul
0	0	0	0	0	0	0	0	0	0	0	0	0	0	0	0	25	3	2	0	0	0	0	0	0	0	0	0	0	0	p = ps_10u_6ul
0	0	0	0	0	0	0	0	0	0	0	0	0	0	0	4	24	2	0	0	0	0	0	0	0	0	0	0	0	0	q = ps_10u_7ul
0	0	0	0	0	0	0	0	0	0	0	1	0	0	0	0	0	23	6	0	0	0	0	0	0	0	0	0	0	0	r = ps_10u_8ul
0	0	0	0	0	0	0	0	0	0	0	0	0	0	0	0	0	1	29	0	0	0	0	0	0	0	0	0	0	0	s = ps_10u_9ul
0	0	0	0	0	0	0	0	0	0	0	0	0	0	0	0	0	0	1	29	0	0	0	0	0	0	0	0	0	0	t = ps_10u_10ul
1	0	2	0	1	0	0	1	1	0	0	0	0	5	0	0	0	0	0	0	8	1	7	3	0	0	0	0	0	0	u = me_1ul
0	0	3	0	1	0	0	0	1	0	1	1	0	0	0	1	0	0	0	0	1	8	1	1	3	3	0	4	1	0	v = me_2ul
0	0	0	1	0	0	0	4	3	0	0	0	0	0	0	0	0	1	2	0	4	1	5	7	1	0	0	1	0	0	w = me_3ul
0	0	0	0	0	0	0	0	4	0	0	0	0	0	0	0	0	1	0	1	0	2	1	3	14	3	0	0	1	0	x = me_4ul
0	0	0	1	0	0	0	0	0	0	0	0	0	0	0	0	1	0	2	1	0	1	1	0	5	9	0	6	2	0	y = me_5ul
0	0	0	0	1	0	0	0	1	0	0	0	0	0	0	0	0	0	1	2	0	0	1	2	2	7	5	1	1	6	z = me_6ul
0	0	0	0	1	0	0	0	0	0	0	0	0	0	0	0	0	0	0	0	0	3	0	2	1	5	10	4	4	0	aa = me_7ul
0	0	0	0	2	1	0	0	0	1	1	0	0	0	0	0	0	0	0	0	0	3	3	1	1	1	6	0	8	2	ab = me_8ul
0	0	0	0	2	1	0	0	0	0	0	0	0	0	0	0	0	0	2	0	1	0	0	2	1	0	7	5	6	3	ac = me_9ul
0	0	0	0	0	0	0	0	0	0	0	0	0	0	0	2	0	0	0	0	3	1	2	2	0	0	0	4	4	12	ad = me_10ul

Fig. 19. Confusion matrix of concentration-dependent classification results for microplastics using 10-fold cross validation with top 10 features selected.

a	b	c	d	e	f	g	h	i	j	k	l	m	n	o	p	q	r	s	t	u	v	w	x	y	z	aa	ab	ac	ad	<-- classified as
8	0	0	0	0	0	0	2	0	0	0	0	0	0	0	0	0	0	0	0	0	0	0	0	0	0	0	0	0	0	a = ps_8u_1ul
0	7	0	1	2	0	0	0	0	0	0	0	0	0	0	0	0	0	0	0	0	0	0	0	0	0	0	0	0	0	b = ps_8u_2ul
0	4	3	3	0	0	1	0	1	0	0	0	0	0	0	0	0	0	0	0	0	0	0	0	0	0	0	0	0	0	c = ps_8u_3ul
0	0	0	5	0	0	0	0	0	0	0	0	0	0	0	0	0	0	0	0	0	0	0	0	0	0	0	0	0	0	d = ps_8u_4ul
0	0	0	1	5	0	0	1	0	0	0	0	0	0	0	0	0	0	0	0	0	0	0	0	0	0	0	0	0	0	e = ps_8u_5ul
0	0	0	0	1	0	0	8	4	1	0	0	0	0	0	0	0	0	0	0	0	0	0	0	0	0	0	0	0	0	f = ps_8u_6ul
0	0	0	0	1	0	0	2	8	0	0	0	0	0	0	0	0	0	0	0	0	0	0	0	0	0	0	0	0	0	g = ps_8u_7ul
0	0	0	1	0	0	0	7	0	0	0	0	0	0	0	0	0	0	0	0	0	0	0	0	0	0	0	0	0	0	h = ps_8u_8ul
0	0	0	0	1	0	0	0	4	4	0	0	0	0	0	0	0	0	0	0	0	0	0	0	0	0	0	0	0	0	i = ps_8u_9ul
0	0	0	0	0	0	0	0	0	10	0	0	0	0	0	0	0	0	0	0	0	0	0	0	0	0	0	0	0	0	j = ps_8u_10ul
0	0	0	0	0	0	0	0	0	0	6	0	0	0	0	0	0	0	0	0	0	0	0	0	0	0	0	0	0	0	k = ps_10u_1ul
0	0	0	0	0	0	0	0	0	0	1	11	0	0	0	0	0	0	0	0	0	0	0	0	0	0	0	0	0	0	l = ps_10u_2ul
0	0	0	0	0	0	0	0	0	0	0	0	13	0	0	0	0	0	0	0	0	0	0	0	0	0	0	0	0	0	m = ps_10u_3ul
0	0	1	2	0	0	0	0	0	0	2	0	0	4	0	2	0	0	0	0	0	0	0	0	0	0	0	0	0	0	n = ps_10u_4ul
0	0	0	0	0	0	0	0	0	0	0	0	0	0	3	3	0	2	0	1	0	0	0	0	0	0	0	0	0	0	o = ps_10u_5ul
0	0	0	0	0	0	0	0	0	0	0	0	0	0	0	9	2	0	0	0	0	0	0	0	0	0	0	0	0	0	p = ps_10u_6ul
0	0	0	0	0	0	0	0	0	0	1	0	0	0	0	0	6	0	1	0	0	0	0	0	0	0	0	0	0	0	q = ps_10u_7ul
0	0	0	0	0	0	0	0	0	0	0	1	0	0	0	0	0	7	0	0	0	0	0	0	0	0	0	0	0	0	r = ps_10u_8ul
0	0	0	0	0	0	0	0	0	0	0	0	0	0	0	0	0	2	6	0	0	0	0	0	0	0	0	0	0	0	s = ps_10u_9ul
0	0	0	0	0	0	0	0	0	0	0	0	0	0	0	0	0	0	0	13	0	0	0	0	0	0	0	0	0	0	t = ps_10u_10ul
0	0	0	0	0	0	0	2	0	0	0	0	0	1	0	0	0	0	0	0	2	0	0	2	0	0	0	0	1	0	u = me_1ul
0	0	2	0	1	0	0	0	0	0	1	0	3	0	0	0	0	0	0	0	1	1	0	1	1	1	0	0	0	0	v = me_2ul
0	0	0	0	0	0	0	2	0	0	0	0	0	0	0	0	0	0	0	0	3	0	1	0	0	0	0	1	0	1	w = me_3ul
0	0	0	0	4	0	0	0	1	0	0	0	0	0	0	0	0	0	0	0	1	4	0	0	0	0	0	0	0	0	x = me_4ul
0	0	0	1	0	0	0	0	0	0	0	0	0	0	0	0	0	1	0	0	1	0	0	5	1	0	2	0	0	1	y = me_5ul
0	0	0	1	0	0	0	0	0	0	0	0	0	0	0	1	1	0	0	0	0	0	1	2	0	0	5	1	1	1	z = me_6ul
0	0	0	0	1	0	0	0	0	0	0	0	0	0	0	0	0	0	0	0	0	0	1	1	0	4	2	0	0	0	aa = me_7ul
0	0	0	0	2	0	0	0	0	0	0	0	0	0	0	0	0	0	0	0	1	0	0	0	1	0	1	1	3	0	ab = me_8ul
0	0	1	0	0	1	0	0	0	0	0	0	0	0	0	1	0	2	0	0	1	0	0	2	0	2	0	2	1	0	ac = me_9ul
0	0	0	0	0	0	0	0	0	0	0	0	0	0	0	1	0	0	0	0	1	0	0	0	0	1	0	2	2	3	ad = me_10ul

Fig. 20. Confusion matrix of concentration-dependent classification results for microplastics using 66 % training and 33 % test data with top 10 features selected.

a	b	c	d	e	f	g	h	i	j	k	l	m	n	o	p	q	r	s	t	u	v	w	x	<-- classified as
29	0	0	0	0	0	0	0	0	0	0	0	0	0	0	0	0	0	0	0	1	0	0	0	a = 25ppm_as
0	30	0	0	0	0	0	0	0	0	0	0	0	0	0	0	0	0	0	0	0	0	0	0	b = 50ppm_as
1	0	20	0	0	0	0	0	0	0	0	0	0	0	0	0	2	2	1	0	0	4	0	0	c = 100ppm_as
0	0	0	27	0	0	0	0	0	0	0	0	0	0	0	0	2	0	0	0	0	1	0	0	d = 25ppm_cd
1	2	0	1	25	0	1	0	0	0	0	0	0	0	0	0	0	0	0	0	0	0	0	0	e = 50ppm_cd
0	0	0	0	0	20	2	0	0	2	1	0	0	0	2	0	0	0	0	2	0	0	1	0	f = 100ppm_cd
2	1	3	0	0	0	20	3	0	0	0	0	0	0	0	0	0	0	0	0	0	0	1	0	g = 25ppm_cr
0	0	0	0	0	0	0	30	0	0	0	0	0	0	0	0	0	0	0	0	0	0	0	0	h = 50ppm_cr
0	0	0	0	0	0	0	0	30	0	0	0	0	0	0	0	0	0	0	0	0	0	0	0	i = 100ppm_cr
0	0	0	0	0	0	0	0	0	29	0	0	0	0	0	0	0	0	0	0	0	0	0	1	j = 25ppm_cu
0	0	0	0	0	0	0	0	0	0	28	0	0	0	0	0	0	0	0	0	0	0	2	0	k = 50ppm_cu
0	0	0	0	0	0	0	0	0	0	0	30	0	0	0	0	0	0	0	0	0	0	0	0	l = 100ppm_cu
0	0	0	0	0	0	0	1	0	0	0	0	23	6	0	0	0	0	0	0	0	0	0	0	m = 25ppm_hg
0	0	0	0	1	0	0	0	0	0	0	0	2	25	0	0	0	0	2	0	0	0	0	0	n = 50ppm_hg
0	0	0	0	0	0	0	0	0	0	0	0	0	0	29	0	0	1	0	0	0	0	0	0	o = 100ppm_hg
0	0	0	3	0	0	0	0	0	0	0	0	0	1	0	25	1	0	0	0	0	0	0	0	p = 25ppm_ni
0	0	0	1	0	0	0	0	0	0	0	0	0	0	0	4	22	0	1	2	0	0	0	0	q = 50ppm_ni
1	0	0	3	2	0	0	0	1	0	0	0	2	1	2	2	1	15	0	0	0	0	0	0	r = 100ppm_ni
0	0	0	0	0	0	0	0	0	0	0	0	0	0	0	0	0	0	30	0	0	0	0	0	s = 25ppm_pb
0	2	0	3	0	0	2	0	0	0	1	0	0	0	3	3	4	0	2	9	0	0	1	0	t = 50ppm_pb
0	0	0	1	2	0	0	0	0	0	0	0	0	0	0	0	0	0	0	2	24	0	0	1	u = 100ppm_pb
0	3	0	0	0	0	3	2	0	0	0	0	2	0	0	1	0	0	0	0	1	16	2	0	v = 25ppm_zn
0	0	0	0	0	0	0	0	0	1	2	0	0	0	0	0	0	0	0	0	0	0	27	0	w = 50ppm_zn
0	0	2	0	0	0	0	0	0	0	0	0	0	0	0	0	0	0	0	0	0	0	0	28	x = 100ppm_zn

Fig. 21. Confusion matrix of concentration-dependent classification results for heavy metals using 10-fold cross validation with top 10 features selected.

a	b	c	d	e	f	g	h	i	j	k	l	m	n	o	p	q	r	s	t	u	v	w	x	<-- classified as
8	0	0	0	0	0	0	0	0	0	0	0	0	0	0	0	0	0	0	0	0	0	0	0	a = 25ppm_as
0	9	0	0	0	0	0	0	0	0	0	0	0	0	0	0	0	0	0	0	0	0	0	0	b = 50ppm_as
0	0	8	0	0	0	0	0	0	0	0	0	0	0	0	2	1	0	0	0	0	0	0	0	c = 100ppm_as
0	0	0	15	0	0	0	0	0	0	0	0	0	0	0	0	0	0	0	0	0	0	0	0	d = 25ppm_cd
0	0	0	1	9	0	0	0	0	0	0	0	0	0	0	0	0	0	0	0	0	0	0	0	e = 50ppm_cd
0	0	0	0	0	8	0	0	0	1	0	0	0	0	1	0	0	0	0	0	0	0	0	0	f = 100ppm_cd
1	1	0	0	0	0	4	0	0	0	0	0	0	0	0	0	0	0	0	0	0	0	0	1	g = 25ppm_cr
0	0	0	0	0	0	0	8	0	0	0	0	0	0	0	0	0	0	0	0	0	0	0	0	h = 50ppm_cr
0	0	0	0	0	0	0	0	13	0	0	0	0	0	0	0	0	0	0	0	0	0	0	0	i = 100ppm_cr
0	0	0	0	0	0	0	0	0	11	0	0	0	0	0	0	0	0	0	0	0	0	0	0	j = 25ppm_cu
0	0	0	0	0	0	0	0	0	0	10	0	0	0	0	0	0	0	0	0	0	0	0	0	k = 50ppm_cu
0	0	0	0	0	0	0	0	0	0	0	11	0	0	0	0	0	0	0	0	0	0	0	0	l = 100ppm_cu
0	0	0	0	0	0	0	1	0	0	0	0	10	1	0	0	0	1	0	0	0	0	0	0	m = 25ppm_hg
0	0	0	0	0	0	0	0	0	0	0	0	2	7	0	0	0	0	1	0	0	0	0	0	n = 50ppm_hg
0	0	0	1	0	0	0	0	0	0	0	0	0	0	8	0	0	0	0	0	0	0	0	0	o = 100ppm_hg
0	0	0	0	0	0	0	0	0	0	0	0	0	0	0	8	0	0	0	0	0	0	0	0	p = 25ppm_ni
0	0	0	0	0	0	0	0	0	0	0	0	3	0	0	4	7	0	0	1	0	0	0	0	q = 50ppm_ni
1	0	0	0	0	0	0	0	0	0	0	0	0	0	0	1	0	2	0	0	0	0	0	0	r = 100ppm_ni
0	0	0	0	0	0	0	0	0	0	0	0	0	0	0	0	0	0	8	0	0	0	0	0	s = 25ppm_pb
0	0	0	0	0	0	1	0	0	0	0	0	0	0	3	0	0	0	4	3	0	0	0	0	t = 50ppm_pb
0	0	0	2	5	0	0	0	0	0	0	0	0	0	0	1	0	0	0	0	1	0	0	0	u = 100ppm_pb
0	3	0	0	0	0	0	0	0	0	0	0	0	0	0	0	0	0	0	0	0	5	0	0	v = 25ppm_zn
0	1	0	0	0	0	0	0	0	0	4	0	0	0	1	0	0	0	0	0	0	0	6	0	w = 50ppm_zn
0	0	0	0	0	0	0	0	0	0	0	0	0	0	0	0	0	0	0	0	0	0	0	0	10	x = 100ppm_zn

Fig. 22. Confusion matrix of concentration-dependent classification results for heavy metals using 66 % training and 33 % test data with top 10 features selected.

a	b	c	d	e	f	g	h	i	j	k	<-- classified as
292	0	3	0	3	0	0	1	1	0	0	a = ps_8u
0	282	16	0	0	0	0	2	0	0	0	b = ps_10u
10	9	280	0	0	1	0	0	0	0	0	c = me_8u
0	0	0	69	5	4	0	0	3	9	0	d = as
1	0	3	5	63	1	1	5	1	9	1	e = cd
0	0	0	6	0	81	0	0	2	0	1	f = cr
0	0	0	0	0	0	81	0	0	0	9	g = cu
1	0	0	10	13	0	0	63	3	0	0	h = hg
0	0	0	0	11	1	0	4	71	3	0	i = ni
2	0	0	7	11	1	0	6	10	52	1	j = pb
0	0	0	7	0	2	21	3	4	0	53	k = zn

Fig. 23. Confusion matrix of concentration-independent classification results for combined data using 10-fold cross validation with top 10 features selected.

a	b	c	d	e	f	g	h	i	j	k	<-- classified as
103	6	2	0	0	0	0	0	1	0	1	a = ps_8u
0	99	4	0	0	0	0	0	0	0	0	b = ps_10u
5	2	92	0	0	0	0	0	0	0	0	c = me_8u
0	0	0	26	0	0	0	0	0	2	0	d = as
0	0	0	0	16	0	0	5	1	8	0	e = cd
0	0	0	2	0	22	0	0	1	3	0	f = cr
0	0	0	0	0	0	25	0	0	0	1	g = cu
0	0	0	0	2	0	0	28	0	0	0	h = hg
0	0	0	1	5	1	0	0	21	0	0	i = ni
1	0	0	5	1	0	0	3	5	16	0	j = pb
0	0	0	3	0	0	8	0	0	0	13	k = zn

Fig. 24. Confusion matrix of concentration-independent classification results for combined data using 66 % training and 33 % test data with top 10 features selected.

a	b	c	<-- classified as
298	0	2	a = ps_8u
0	286	14	b = ps_10u
4	20	276	c = me_8u

Fig. 25. Confusion matrix of concentration-independent classification results for microplastics using 10-fold cross validation with top 10 features selected.

a	b	c	<-- classified as
95	0	1	a = ps_8u
0	96	3	b = ps_10u
3	8	94	c = me_8u

Fig. 26. Confusion matrix of concentration-independent classification results for microplastics using 66 % training and 33 % test data with top 10 features selected.

a	b	c	d	e	f	g	h	<-- classified as
80	1	1	1	0	4	2	1	a = as
8	66	2	0	2	4	7	1	b = cd
7	1	66	0	4	1	4	7	c = cr
0	0	0	82	0	0	0	8	d = cu
0	3	1	1	79	5	0	1	e = hg
0	4	1	0	5	73	5	2	f = ni
4	5	5	1	4	3	68	0	g = pb
3	1	4	10	1	1	0	70	h = zn

Fig. 27. Confusion matrix of concentration-independent classification results for heavy metals using 10-fold cross validation with top 10 features selected.

a	b	c	d	e	f	g	h	<-- classified as
26	0	0	0	0	0	2	0	a = as
4	28	0	0	0	0	3	0	b = cd
0	0	27	0	0	0	1	0	c = cr
0	0	0	28	0	0	0	4	d = cu
0	1	0	0	31	0	0	0	e = hg
2	3	0	0	0	17	5	0	f = ni
0	0	0	0	3	0	25	0	g = pb
4	0	1	3	4	0	0	18	h = zn

Fig. 28. Confusion matrix of concentration-independent classification results for heavy metals using 66 % training and 33 % test data with top 10 features selected.

Fig. 29. Confusion matrix of concentration-dependent classification results for combined data using 10-fold cross validation with top 20 features selected.

Fig. 30. Confusion matrix of concentration-dependent classification results for combined data using 66 % training and 33 % test data with top 20 features selected.

a	b	c	d	e	f	g	h	i	j	k	l	m	n	o	p	q	r	s	t	u	v	w	x	y	z	aa	ab	ac	ad	<-- classified as
27	0	0	3	0	0	0	0	0	0	0	0	0	0	0	0	0	0	0	0	0	0	0	0	0	0	0	0	0	0	a = ps_8u_1ul
0	20	0	1	3	0	0	0	0	0	0	0	0	0	0	0	0	0	0	0	0	0	0	4	2	0	0	0	0	0	b = ps_8u_2ul
0	1	16	8	1	0	0	0	1	0	0	0	0	0	1	0	1	0	0	0	0	0	0	1	0	0	0	0	0	0	c = ps_8u_3ul
0	0	5	13	3	3	0	2	1	0	0	0	0	0	0	0	1	0	0	0	0	0	0	0	2	0	0	0	0	0	d = ps_8u_4ul
0	0	1	3	20	3	0	0	1	2	0	0	0	0	0	0	0	0	0	0	0	0	0	0	0	0	0	0	0	0	e = ps_8u_5ul
0	0	0	5	0	16	5	1	1	1	0	0	0	0	0	0	0	0	0	0	0	1	0	0	0	0	0	0	0	0	f = ps_8u_6ul
0	0	0	0	2	7	20	0	1	0	0	0	0	0	0	0	0	0	0	0	0	0	0	0	0	0	0	0	0	0	g = ps_8u_7ul
2	0	0	3	1	4	3	15	0	0	0	0	0	0	0	0	0	0	0	0	0	1	0	0	0	0	1	0	0	0	h = ps_8u_8ul
0	0	0	0	0	0	0	2	20	8	0	0	0	0	0	0	0	0	0	0	0	0	0	0	0	0	0	0	0	0	i = ps_8u_9ul
0	0	0	0	0	0	0	0	0	30	0	0	0	0	0	0	0	0	0	0	0	0	0	0	0	0	0	0	0	0	j = ps_8u_10ul
0	0	0	0	0	0	0	0	0	0	29	0	0	0	0	0	0	0	0	0	1	0	0	0	0	0	0	0	0	0	k = ps_10u_1ul
0	0	0	0	0	0	0	0	0	0	0	30	0	0	0	0	0	0	0	0	0	0	0	0	0	0	0	0	0	0	l = ps_10u_2ul
0	0	0	0	0	0	0	0	0	0	0	0	30	0	0	0	0	0	0	0	0	0	0	0	0	0	0	0	0	0	m = ps_10u_3ul
0	0	0	0	0	0	0	0	0	0	0	0	0	28	0	0	0	0	0	0	0	0	1	0	1	0	0	0	0	0	n = ps_10u_4ul
0	0	0	0	0	0	0	0	0	0	1	0	0	1	18	8	0	0	0	0	0	0	2	0	0	0	0	0	0	0	o = ps_10u_5ul
0	0	0	0	0	0	0	0	0	0	0	1	0	0	0	0	28	0	1	0	0	0	0	0	0	0	0	0	0	0	p = ps_10u_6ul
0	0	0	0	0	0	0	0	0	0	2	0	0	2	2	0	22	2	0	0	0	0	0	0	0	0	0	0	0	0	q = ps_10u_7ul
0	0	0	0	0	0	0	0	0	0	0	0	0	0	0	0	0	30	0	0	0	0	0	0	0	0	0	0	0	0	r = ps_10u_8ul
0	0	0	0	0	0	0	0	0	0	0	0	0	0	0	0	0	1	0	28	1	0	0	0	0	0	0	0	0	0	s = ps_10u_9ul
0	0	0	0	0	0	0	0	0	0	0	0	0	0	0	0	0	0	0	0	30	0	0	0	0	0	0	0	0	0	t = ps_10u_10ul
0	2	0	0	0	0	0	0	0	1	0	0	0	0	1	2	0	0	0	11	0	1	6	0	1	1	4	0	0	0	u = me_1ul
0	0	0	2	0	0	0	0	0	0	1	1	3	1	0	0	0	0	0	0	1	6	1	2	2	3	1	4	0	2	v = me_2ul
0	0	0	0	0	0	1	0	0	0	0	0	0	0	0	0	0	1	1	0	0	1	22	0	1	2	1	0	0	0	w = me_3ul
0	1	0	0	0	0	2	0	0	0	0	0	0	0	0	0	0	1	1	0	0	2	7	9	5	0	0	1	0	0	x = me_4ul
0	0	0	1	0	0	0	0	0	0	0	0	0	1	1	0	0	1	0	0	0	1	4	2	14	1	2	2	0	0	y = me_5ul
0	0	0	0	0	0	0	0	0	0	0	0	0	0	0	0	0	0	0	0	0	2	1	1	3	1	11	3	6	0	2	z = me_6ul
0	0	0	0	0	0	0	0	0	0	0	0	0	0	0	0	0	0	0	0	0	1	0	0	3	1	1	14	6	3	1	aa = me_7ul
0	0	0	0	1	0	0	0	0	0	0	0	0	0	0	0	0	0	0	0	0	1	2	1	3	1	2	0	11	8	0	ab = me_8ul
0	0	0	0	0	1	0	0	0	0	0	0	0	0	0	0	0	0	0	0	0	3	0	2	0	2	2	5	10	5	ac = me_9ul
0	0	0	0	0	0	0	0	0	0	0	0	1	0	0	0	0	1	0	0	2	0	1	2	0	0	1	1	5	16	ad = me_10ul

Fig. 31. Confusion matrix of concentration-dependent classification results for microplastics using 10-fold cross validation with top 20 features selected.

a	b	c	d	e	f	g	h	i	j	k	l	m	n	o	p	q	r	s	t	u	v	w	x	y	z	aa	ab	ac	ad	<-- classified as
9	0	0	0	0	0	0	1	0	0	0	0	0	0	0	0	0	0	0	0	0	0	0	0	0	0	0	0	0	0	a = ps_8u_1ul
0	7	1	1	1	0	0	0	0	0	0	0	0	0	0	0	0	0	0	0	0	0	0	0	0	0	0	0	0	0	b = ps_8u_2ul
0	0	3	3	0	1	2	0	3	0	0	0	0	0	0	0	0	0	0	0	0	0	0	0	0	0	0	0	0	0	c = ps_8u_3ul
0	0	0	1	0	0	0	4	0	0	0	0	0	0	0	0	0	0	0	0	0	0	0	0	0	0	0	0	0	0	d = ps_8u_4ul
0	0	0	1	5	0	0	0	0	1	0	0	0	0	0	0	0	0	0	0	0	0	0	0	0	0	0	0	0	0	e = ps_8u_5ul
0	0	0	0	1	3	1	3	0	6	0	0	0	0	0	0	0	0	0	0	0	0	0	0	0	0	0	0	0	0	f = ps_8u_6ul
0	0	0	0	0	0	3	0	2	6	0	0	0	0	0	0	0	0	0	0	0	0	0	0	0	0	0	0	0	0	g = ps_8u_7ul
0	0	0	0	0	0	3	5	0	0	0	0	0	0	0	0	0	0	0	0	0	0	0	0	0	0	0	0	0	0	h = ps_8u_8ul
0	0	0	0	0	0	0	0	5	4	0	0	0	0	0	0	0	0	0	0	0	0	0	0	0	0	0	0	0	0	i = ps_8u_9ul
0	0	0	0	0	0	0	0	0	0	10	0	0	0	0	0	0	0	0	0	0	0	0	0	0	0	0	0	0	0	j = ps_8u_10ul
0	0	0	0	0	0	0	0	0	0	5	0	0	0	0	0	0	0	0	0	1	0	0	0	0	0	0	0	0	0	k = ps_10u_1ul
0	0	0	0	0	0	0	0	0	0	0	1	11	0	0	0	0	0	0	0	0	0	0	0	0	0	0	0	0	0	l = ps_10u_2ul
0	0	0	0	0	0	0	0	0	0	0	0	13	0	0	0	0	0	0	0	0	0	0	0	0	0	0	0	0	0	m = ps_10u_3ul
0	0	0	0	0	0	0	0	0	0	2	0	0	9	0	0	0	0	0	0	0	0	0	0	0	0	0	0	0	0	n = ps_10u_4ul
0	0	0	0	0	0	0	0	0	0	0	0	0	0	3	3	1	0	1	0	1	0	0	0	0	0	0	0	0	0	o = ps_10u_5ul
0	0	0	0	0	0	0	0	0	0	0	0	0	0	0	0	11	0	0	0	0	0	0	0	0	0	0	0	0	0	p = ps_10u_6ul
0	0	0	0	0	0	0	0	0	0	1	0	0	0	0	0	6	1	0	0	0	0	0	0	0	0	0	0	0	0	q = ps_10u_7ul
0	0	0	0	0	0	0	0	0	0	0	0	0	0	0	0	0	8	0	0	0	0	0	0	0	0	0	0	0	0	r = ps_10u_8ul
0	0	0	0	0	0	0	0	0	0	0	0	0	0	0	0	1	1	6	0	0	0	0	0	0	0	0	0	0	0	s = ps_10u_9ul
0	0	0	0	0	0	0	0	0	0	0	0	0	0	0	0	0	0	0	13	0	0	0	0	0	0	0	0	0	0	t = ps_10u_10ul
0	1	0	0	0	0	0	0	0	0	0	0	0	0	0	0	1	0	1	0	5	0	0	0	0	0	0	0	0	0	u = me_1ul
0	0	2	3	0	0	0	0	0	0	1	0	3	0	0	0	0	0	0	0	0	1	0	0	1	0	0	1	0	0	v = me_2ul
0	0	0	0	0	0	0	0	0	0	0	0	0	0	0	0	0	0	0	0	0	0	1	2	0	0	0	5	0	0	w = me_3ul
0	0	0	0	0	0	0	0	0	0	0	0	0	1	0	0	0	0	0	0	0	1	0	6	1	0	0	1	0	0	x = me_4ul
0	0	0	0	0	0	0	1	0	0	0	0	0	0	0	0	0	0	0	0	0	0	0	7	1	2	1	0	0	0	y = me_5ul
0	0	0	1	0	0	0	0	0	0	0	0	0	1	0	0	0	0	0	0	0	0	0	1	0	0	6	3	0	2	z = me_6ul
0	0	0	0	0	0	0	0	0	0	0	0	0	0	0	0	0	0	0	0	0	0	0	1	0	1	4	2	1	0	aa = me_7ul
0	1	0	2	0	0	0	0	0	0	0	0	0	0	0	0	0	0	0	0	0	0	0	1	0	0	4	1	0	0	ab = me_8ul
0	0	0	0	0	0	0	0	1	0	0	0	0	0	0	0	0	0	0	0	1	0	0	2	0	0	5	3	1	0	ac = me_9ul
0	0	0	0	0	0	0	0	0	0	0	0	0	0	0	0	0	0	0	0	2	0	0	0	0	1	0	0	2	5	ad = me_10ul

Fig. 32. Confusion matrix of concentration-dependent classification results for microplastics using 66 % training and 33 % test data with top 20 features selected.

a	b	c	d	e	f	g	h	i	j	k	l	m	n	o	p	q	r	s	t	u	v	w	x	<-- classified as
29	0	1	0	0	0	0	0	0	0	0	0	0	0	0	0	0	0	0	0	0	0	0	0	a = 25ppm_as
0	30	0	0	0	0	0	0	0	0	0	0	0	0	0	0	0	0	0	0	0	0	0	0	b = 50ppm_as
0	0	23	0	0	0	0	0	0	0	1	0	0	0	0	0	4	0	0	1	1	0	0	0	c = 100ppm_as
0	0	0	29	0	0	0	0	0	0	0	0	0	0	0	0	0	0	0	0	1	0	0	0	d = 25ppm_cd
0	2	0	0	26	0	2	0	0	0	0	0	0	0	0	0	0	0	0	0	0	0	0	0	e = 50ppm_cd
0	0	0	0	0	20	0	0	0	1	0	0	0	0	0	0	0	0	1	6	0	0	0	2	f = 100ppm_cd
4	3	0	0	0	0	20	2	0	0	0	0	0	0	0	0	0	0	0	1	0	0	0	0	g = 25ppm_cr
0	0	0	0	0	0	0	30	0	0	0	0	0	0	0	0	0	0	0	0	0	0	0	0	h = 50ppm_cr
0	0	0	0	0	0	0	0	30	0	0	0	0	0	0	0	0	0	0	0	0	0	0	0	i = 100ppm_cr
0	0	0	0	0	0	0	0	0	30	0	0	0	0	0	0	0	0	0	0	0	0	0	0	j = 25ppm_cu
0	0	0	0	0	0	0	0	0	0	22	1	0	0	0	0	0	0	0	0	0	0	5	2	k = 50ppm_cu
0	0	0	0	0	0	0	0	0	0	0	30	0	0	0	0	0	0	0	0	0	0	0	0	l = 100ppm_cu
0	0	0	0	0	0	0	0	0	0	0	0	28	1	0	0	0	1	0	0	0	0	0	0	m = 25ppm_hg
0	0	0	0	0	0	0	0	0	1	0	0	0	0	26	0	0	1	0	2	0	0	0	0	n = 50ppm_hg
0	0	0	1	4	0	0	0	1	0	0	0	0	2	20	0	1	1	0	0	0	0	0	0	o = 100ppm_hg
0	0	2	3	0	3	0	0	0	0	0	0	0	1	0	20	0	1	0	0	0	0	0	0	p = 25ppm_ni
0	0	0	0	0	0	0	0	0	0	0	0	0	0	0	0	5	21	0	3	1	0	0	0	q = 50ppm_ni
1	0	0	1	0	0	0	1	0	0	0	0	2	0	0	0	1	23	0	1	0	0	0	0	r = 100ppm_ni
0	0	0	0	0	0	0	0	0	0	0	0	0	0	0	0	0	0	30	0	0	0	0	0	s = 25ppm_pb
0	0	0	0	0	1	1	0	0	0	2	0	0	0	0	2	5	0	4	10	3	0	0	2	t = 50ppm_pb
0	0	0	0	2	0	0	0	0	0	0	0	0	0	0	0	0	0	0	4	24	0	0	0	u = 100ppm_pb
0	1	0	0	0	0	2	0	0	0	2	0	3	0	2	0	1	0	0	1	2	12	3	1	v = 25ppm_zn
0	0	0	0	0	0	0	0	0	0	1	0	0	0	0	0	0	0	0	0	0	0	29	0	w = 50ppm_zn
0	0	3	0	0	0	0	0	0	1	0	0	0	0	0	0	0	0	0	0	0	0	2	24	x = 100ppm_zn

Fig. 33. Confusion matrix of concentration-dependent classification results for heavy metals using 10-fold cross validation with top 10 features selected.

a	b	c	d	e	f	g	h	i	j	k	l	m	n	o	p	q	r	s	t	u	v	w	x	<-- classified as
4	0	3	0	0	0	0	0	0	0	0	0	0	0	0	0	1	0	0	0	0	0	0	0	a = 25ppm_as
0	9	0	0	0	0	0	0	0	0	0	0	0	0	0	0	0	0	0	0	0	0	0	0	b = 50ppm_as
0	0	11	0	0	0	0	0	0	0	0	0	0	0	0	0	0	0	0	0	0	0	0	0	c = 100ppm_as
0	0	0	15	0	0	0	0	0	0	0	0	0	0	0	0	0	0	0	0	0	0	0	0	d = 25ppm_cd
3	1	0	2	2	0	0	0	0	0	0	0	0	1	0	0	0	0	0	0	1	0	0	0	e = 50ppm_cd
0	0	0	0	0	8	0	0	0	2	0	0	0	0	0	0	0	0	0	0	0	0	0	0	f = 100ppm_cd
0	0	0	0	0	0	4	1	0	0	0	0	0	0	0	0	0	0	1	0	0	1	0	0	g = 25ppm_cr
0	0	0	0	0	0	0	8	0	0	0	0	0	0	0	0	0	0	0	0	0	0	0	0	h = 50ppm_cr
0	0	0	0	0	0	0	0	13	0	0	0	0	0	0	0	0	0	0	0	0	0	0	0	i = 100ppm_cr
0	0	0	0	0	0	0	0	0	11	0	0	0	0	0	0	0	0	0	0	0	0	0	0	j = 25ppm_cu
0	0	0	0	0	0	0	0	0	3	6	1	0	0	0	0	0	0	0	0	0	0	0	0	k = 50ppm_cu
0	0	0	0	0	0	0	0	0	0	0	11	0	0	0	0	0	0	0	0	0	0	0	0	l = 100ppm_cu
0	0	0	0	0	0	0	0	0	0	0	0	13	0	0	0	0	0	0	0	0	0	0	0	m = 25ppm_hg
0	0	0	0	0	0	0	0	0	0	0	0	0	10	0	0	0	0	0	0	0	0	0	0	n = 50ppm_hg
0	0	0	2	0	0	0	0	0	0	0	0	0	0	6	0	0	1	0	0	0	0	0	0	o = 100ppm_hg
0	0	0	3	0	1	0	0	0	0	0	0	0	0	0	4	0	0	0	0	0	0	0	0	p = 25ppm_ni
0	0	0	0	0	0	0	0	0	0	0	0	0	0	0	0	2	9	1	2	1	0	0	0	q = 50ppm_ni
0	0	0	0	0	0	0	0	0	0	0	0	0	0	0	0	0	2	2	0	0	0	0	0	r = 100ppm_ni
0	0	0	0	0	0	0	0	0	0	0	0	0	0	0	0	0	0	8	0	0	0	0	0	s = 25ppm_pb
0	0	0	0	0	0	1	0	0	3	0	0	0	0	0	0	0	0	4	3	0	0	0	0	t = 50ppm_pb
0	0	0	2	0	0	3	0	0	0	0	0	0	0	0	0	0	0	1	0	1	0	2	0	u = 100ppm_pb
0	1	0	0	0	0	0	0	0	0	0	0	0	0	2	0	0	0	0	0	0	5	0	0	v = 25ppm_zn
0	5	0	0	0	0	0	0	0	0	0	0	0	0	0	0	0	0	0	0	0	0	6	1	w = 50ppm_zn
0	0	0	0	0	0	0	0	0	0	0	0	0	0	0	0	0	0	0	0	0	0	2	8	x = 100ppm_zn

Fig. 34. Confusion matrix of concentration-dependent classification results for heavy metals using 66 % training and 33 % test data with top 20 features selected.

a	b	c	d	e	f	g	h	i	j	k	<-- classified as
297	1	1	0	0	0	1	0	0	0	0	a = ps_8u
0	297	3	0	0	0	0	0	0	0	0	b = ps_10u
9	7	284	0	0	0	0	0	0	0	0	c = me_8u
0	0	0	75	3	1	1	0	2	5	3	d = as
0	0	0	7	70	0	0	1	4	7	1	e = cd
0	0	0	7	0	81	0	0	2	0	0	f = cr
0	0	0	0	0	0	77	0	0	0	13	g = cu
0	0	0	3	7	0	0	79	0	0	1	h = hg
0	0	0	2	8	4	0	2	72	2	0	i = ni
2	0	0	7	8	0	0	5	5	62	1	j = pb
0	0	0	4	0	2	14	3	1	0	66	k = zn

Fig. 35. Confusion matrix of concentration-independent classification results for combined data using 10-fold cross validation with top 20 features selected.

a	b	c	d	e	f	g	h	i	j	k	<-- classified as
110	1	0	0	0	0	0	2	0	0	0	a = ps_8u
0	103	0	0	0	0	0	0	0	0	0	b = ps_10u
0	3	95	0	0	0	0	1	0	0	0	c = me_8u
0	0	0	27	1	0	0	0	0	0	0	d = as
0	0	0	1	23	0	0	0	0	6	0	e = cd
1	0	0	0	0	26	0	0	1	0	0	f = cr
0	0	0	0	0	0	19	0	0	0	7	g = cu
0	0	0	0	5	0	0	24	1	0	0	h = hg
0	0	0	0	4	0	0	0	24	0	0	i = ni
0	0	0	3	3	0	0	1	3	21	0	j = pb
0	0	0	2	0	1	0	0	0	0	21	k = zn

Fig. 36. Confusion matrix of concentration-independent classification results for combined data using 66 % training and 33 % test data with top 20 features selected.

a	b	c	<-- classified as
296	1	3	a = ps_8u
0	298	2	b = ps_10u
3	9	288	c = me_8u

Fig. 37. Confusion matrix of concentration-independent classification results for microplastics using 10-fold cross validation with top 20 features selected.

a	b	c	<-- classified as
95	0	1	a = ps_8u
0	97	2	b = ps_10u
3	2	100	c = me_8u

Fig. 38. Confusion matrix of concentration-independent classification results for microplastics using 66 % training and 33 % test data with top 20 features selected.

a	b	c	d	e	f	g	h	<-- classified as
80	1	0	0	0	4	4	1	a = as
4	78	0	0	0	2	4	2	b = cd
4	0	77	0	2	4	2	1	c = cr
0	0	0	89	0	0	0	1	d = cu
0	4	0	0	82	3	0	1	e = hg
1	1	0	0	2	85	1	0	f = ni
0	2	0	0	0	2	86	0	g = pb
1	1	1	2	0	0	0	85	h = zn

Fig. 39. Confusion matrix of concentration-independent classification results for heavy metals using 10-fold cross validation with top 20 features selected.

a	b	c	d	e	f	g	h	<-- classified as
27	1	0	0	0	0	0	0	a = as
0	35	0	0	0	0	0	0	b = cd
1	0	24	0	0	1	2	0	c = cr
0	0	0	32	0	0	0	0	d = cu
0	3	0	0	27	2	0	0	e = hg
1	2	0	0	0	23	1	0	f = ni
0	1	0	0	0	0	27	0	g = pb
0	0	0	0	0	0	0	30	h = zn

Fig. 40. Confusion matrix of concentration-independent classification results for heavy metals using 66 % training and 33 % test data with top 20 features selected.

```
Ranked attributes:
 1.64936    298 LED16_Photodiode9
 1.64059    204 LED11_Photodiode5
 1.59528    222 LED12_Photodiode5
 1.48933    127 LED7_Photodiode0
 1.48216    146 LED8_Photodiode1
 1.47865    166 LED9_Photodiode3
 1.46264    203 LED11_Photodiode4
 1.45878    128 LED7_Photodiode1
 1.45323    113 LED6_Photodiode4
 1.44696     48 LED2_Photodiode11
```

Fig. 41. Top 10 features identified by feature selection in the combined data sets.

TABLE V. SAMPLE DATA SET.

CLASS	LED16 PD9	LED11 PD5	LED12 PD5	LED7 PD0	LED8 PD1	LED9 PD3	LED11 PD4	LED7 PD1	LED6 PD4	LED2 PD11
ps_8u_10ul	228	1222	501	758	130	316	4096	97	109	575
ps_10u_10ul	184	973	405	517	90	239	3124	66	74	437
me_10ul	160	832	349	483	86	212	2731	62	66	403
50ppm_as	239	1258	514	801	135	329	4224	101	116	585
50ppm_cd	237	1240	506	778	131	319	4141	99	112	595
50ppm_cr	232	1230	504	756	129	322	4138	97	109	599
50ppm_cu	241	1258	515	817	139	331	4191	104	114	596
50ppm_hg	229	1217	498	728	123	307	4068	92	110	580
50ppm_ni	235	1225	499	757	127	313	4074	96	110	580
50ppm_pb	232	1218	496	753	126	310	4062	95	110	578
50ppm_zn	241	1256	513	809	138	330	4184	103	113	575

Note: PD - Photodiode.

VI. DISCUSSION

When the overall performance of the system is evaluated, concentration measurements exhibit a significant dependence on the type of pollutant. Training the network in a concentration-dependent manner for both heavy metals and microplastics increases the error rate. To reduce the error rate, it may be necessary to train the model with a larger number of samples prepared under different conditions, or by utilising a greater number of layers in MLP or deep learning algorithms. In its current form, the system can classify heavy metal types based on concentration with an accuracy of up to 82.08 %. When classifying heavy metals independently of concentration, the system achieves an accuracy of up to 91.94 %. Although the concentration-dependent classification performance for microplastics remains relatively low, the system achieves up to 98 % accuracy in concentration-independent detection. Considering that the samples were prepared at different concentration levels, this performance is deemed acceptable. Furthermore, when the system was assigned to simultaneously classify both microplastics and heavy metals, it achieved an accuracy of 91.29 %. However, these findings also indicate that when introducing new samples, training must be performed with varying concentrations to maintain performance. Confusion matrices are given to show which substance classes are classified more accurately. If a system were designed based on the selected features, it could offer faster decision-making, easier training, lower costs, and improved portability.

Heavy metals and microplastics have distinct properties, which pose challenges for measurement systems. Despite the fact that the microplastics used in this study were micrometer-sized materials, their detection, independent of concentration, achieved high accuracy. For heavy metals, it was observed that, when explicitly operated for concentration measurement, the system provided acceptable accuracy for concentration determination and successfully performed pollutant detection.

ACKNOWLEDGMENT

The authors thank the Proofreading & Editing Office of the Dean for Research at Erciyes University for the copyediting and proofreading service for this manuscript.

CONFLICTS OF INTEREST

The authors declare that they have no conflicts of interest.

REFERENCES

[1] S.-A. Strungaru, R. Jijie, M. Nicoara, G. Plavan, and C. Faggio, “Micro-(nano) plastics in freshwater ecosystems: Abundance, toxicological impact and quantification methodology”, *TrAC Trends in Analytical Chemistry*, vol. 110, pp. 116–128, 2019. DOI: 10.1016/j.trac.2018.10.025.

[2] S. Karbalaei, P. Hanachi, T. R. Walker, and M. Cole, “Occurrence, sources, human health impacts and mitigation of microplastic pollution”, *Environmental Science and Pollution Research*, vol. 25, pp. 36046–36063, 2018. DOI: 10.1007/s11356-018-3508-7.

[3] Y. Zhu, C. H. Yeung, and E. Y. Lam, “Microplastic pollution monitoring with holographic classification and deep learning”, *Journal of Physics: Photonics*, vol. 3, no. 2, pp. 1–12, 2021. DOI: 10.1088/2515-7647/abf250.

[4] W. Li *et al.*, “Effects of environmental and anthropogenic factors on the distribution and abundance of microplastics in freshwater ecosystems”, *Science of The Total Environment*, vol. 856, part 2, art. 159030, 2023. DOI: 10.1016/j.scitotenv.2022.159030.

[5] N. Chang *et al.*, “Unveiling the impacts of microplastic pollution on soil health: A comprehensive review”, *Science of The Total Environment*, vol. 951, art. 175643, 2024. DOI: 10.1016/j.scitotenv.2024.175643.

[6] L. M. Rios Mendoza and M. Balcer, “Microplastics in freshwater environments: A review of quantification assessment”, *TrAC Trends in Analytical Chemistry*, vol. 113, pp. 402–408, 2019. DOI: 10.1016/j.trac.2018.10.020.

[7] T. S. M. Amelia, W. M. A. W. M. Khalik, M. C. Ong, Y. T. Shao, H.-J. Pan, and K. Bhubalan, “Marine microplastics as vectors of major ocean pollutants and its hazards to the marine ecosystem and humans”, *Progress in Earth and Planetary Science*, vol. 8, art. no. 12, 2021. DOI: 10.1186/s40645-020-00405-4.

[8] C. B. Crawford and B. Quinn, *Microplastic Pollutants*. Elsevier, 2016.

[9] H. A. Leslie, "Review of microplastics in cosmetics", Report R14/29, IVM Institute for Environmental Studies, Amsterdam, 2014.

[10] H. S. Auta, C. U. Emenike, and S. H. Fauziah, "Distribution and importance of microplastics in the marine environment: A review of the sources, fate, effects, and potential solutions", *Environment International*, vol. 102, pp. 165–176, 2017. DOI: 10.1016/j.envint.2017.02.013.

[11] M. N. Issac and B. Kandasubramanian, "Effect of microplastics in water and aquatic systems", *Environmental Science and Pollution Research*, vol. 28, pp. 19544–19562, 2021. DOI: 10.1007/s11356-021-13184-2.

[12] M. Zhang, G. Zhu, T. Li, X. Lou, and L. Zhu, "A dual-channel optical fiber sensor based on surface plasmon resonance for heavy metal ions detection in contaminated water", *Optics Communications*, vol. 462, art. 124750, 2020. DOI: 10.1016/j.optcom.2019.124750.

[13] S. Tassone, S. Barbera, H. Kaihara, S. G. Patrucco, and K. Abid, "First evidence of the effects of polyethylene terephthalate microplastics on ruminal degradability and gastro-intestinal digestibility of mixed hay", *Animals*, vol. 14, no. 15, p. 2139, 2024. DOI: 10.3390/ani14152139.

[14] M. Yurtsever, "Possible effects of nano- and microplastics on human health and the ecosystem", *Menba Kastamonu Üniversitesi Su Ürünleri Fakültesi Dergisi*, vol. 5, no. 2, pp. 17–24, 2019.

[15] X. Dong, X. Liu, Q. Hou, and Z. Wang, "From natural environment to animal tissues: A review of microplastics (nanoplastics) translocation and hazards studies", *Science of The Total Environment*, vol. 855, art. 158686, 2023. DOI: 10.1016/j.scitotenv.2022.158686.

[16] S. S. Monteiro *et al.*, "A straightforward method for microplastic extraction from organic-rich freshwater samples", *Science of The Total Environment*, vol. 815, art. 152941, 2022. DOI: 10.1016/j.scitotenv.2022.152941.

[17] K. Kaur *et al.*, "Microplastic-associated pathogens and antimicrobial resistance in environment", *Chemosphere*, vol. 291, part 2, art. 133005, 2022. DOI: 10.1016/j.chemosphere.2021.133005.

[18] S. Pradit, P. Noppradit, B. Goh, K. Sornplang, and M. Ong, and P. Towatana, "Occurrence of microplastics and trace metals in fish and shrimp from Songkhla Lake, Thailand during the Covid-19 pandemic", *Applied Ecology and Environmental Reserach*, vol. 19, pp. 1085–1106, 2021. DOI: 10.15666/aeer/1902_10851106.

[19] B. O. Asamoah, B. Kanyathare, M. Roussey, and K.-E. Peiponen, "A prototype of a portable optical sensor for the detection of transparent and translucent microplastics in freshwater", *Chemosphere*, vol. 231, pp. 161–167, 2019. DOI: 10.1016/j.chemosphere.2019.05.114.

[20] B. E. Oßmann, G. Sarau, H. Holtmannspötter, M. Pischetsrieder, S. H. Christiansen, and W. Dicke, "Small-sized microplastics and pigmented particles in bottled mineral water", *Water Research*, vol. 141, pp. 307–316, 2018. DOI: 10.1016/j.watres.2018.05.027.

[21] A. K. Sharma *et al.*, "A systematic review on assessment of heavy metals toxicity in freshwater fish species: Current scenario and remedial approaches", *Journal of Geochemical Exploration*, vol. 262, art. 107472, 2024. DOI: 10.1016/j.gexplo.2024.107472.

[22] S. Karnchanawong and P. Limpiteeprakan, "Evaluation of heavy metal leaching from spent household batteries disposed in municipal solid waste", *Waste Management*, vol. 29, no. 2, pp. 550–558, 2009. DOI: 10.1016/j.wasman.2008.03.018.

[23] X. Li, "A comparative study on the efficacy of conventional and green chelating agents for soil heavy metal remediation", *Theoretical and Natural Science*, vol. 37, no. 1, pp. 206–215, 2024. DOI: 10.54254/2753-8818/37/20240193.

[24] A. Baruah, A. Sharma, S. Sharma, and R. Nagraik, "An insight into different microplastic detection methods", *International Journal of Environmental Science and Technology*, vol. 19, pp. 5721–5730, 2022. DOI: 10.1007/s13762-021-03384-1.

[25] N. Meyers *et al.*, "Microplastic detection and identification by Nile red staining: Towards a semi-automated, cost- and time-effective technique", *Science of The Total Environment*, vol. 823, art. 153441, 2022. DOI: 10.1016/j.scitotenv.2022.153441.

[26] C. Ompala, J.-P. Renault, O. Taché, É. Cournède, S. Devineau, and C. Chivas-Joly, "Stability and dispersibility of microplastics in experimental exposure medium and their dimensional characterization by SMLS, SAXS, Raman microscopy, and SEM", *Journal of Hazardous Materials*, vol. 469, art. 134083, 2024. DOI: 10.1016/j.jhazmat.2024.134083.

[27] B. A. Newrick, D. Valdés, A. Laca, A. Laca, and M. Díaz, "Enhanced biodegradation of high-density polyethylene microplastics: Study of bacterial efficiency and process parameters", *Journal of Hazardous Materials*, vol. 485, art. 136822, 2025. DOI: 10.1016/j.jhazmat.2024.136822.

[28] L. Rodriguez-Saona, D. P. Aykas, K. R. Borba, and A. U. Urbina, "Miniaturization of optical sensors and their potential for high-throughput screening of foods", *Current Opinion in Food Science*, vol. 31, pp. 136–150, 2020. DOI: 10.1016/j.cofs.2020.04.008.

[29] M. B. Gumpu, S. Sethuraman, U. M. Krishnan, and J. B. B. Rayappan, "A review on detection of heavy metal ions in water - An electrochemical approach", *Sensors Actuators B: Chemical*, vol. 213, pp. 515–533, 2015. DOI: 10.1016/j.snb.2015.02.122.

[30] I. Kabenge *et al.*, "Modelling storm event-based sediment yield and assessing its heavy metal loading: Case of Lake Victoria's Inner Murchison Bay catchment in Uganda", *Modelling Earth Systems and Environment*, vol. 10, no. 2, pp. 1973–1991, 2024. DOI: 10.1007/s40808-023-01876-2.

[31] K. Sadani, P. Nag, and S. Mukherji, "LSPR based optical fiber sensor with chitosan capped gold nanoparticles on BSA for trace detection of Hg (II) in water, soil and food samples", *Biosensensors and Bioelectronics*, vol. 134, pp. 90–96, 2019. DOI: 10.1016/j.bios.2019.03.046.

[32] L. K. Pandey *et al.*, "Assessment of metal contamination in water and sediments from major rivers in South Korea from 2008 to 2015", *Science of The Total Environment*, vol. 651, part 1, pp. 323–333, 2019. DOI: 10.1016/j.scitotenv.2018.09.057.

[33] R. Jain, A. Thakur, P. Kaur, K.-H. Kim, and P. Devi, "Advances in imaging-assisted sensing techniques for heavy metals in water: Trends, challenges, and opportunities", *TrAC Trends in Analytical Chemistry*, vol. 123, art. 115758, 2020. DOI: 10.1016/j.trac.2019.115758.

[34] S. Sajed, F. Arefi, M. Kolahdouz, and M. A. Sadeghi, "Improving sensitivity of mercury detection using learning based smartphone colorimetry", *Sensors and Actuators B: Chemical*, vol. 298, art. 126942, 2019. DOI: 10.1016/j.snb.2019.126942.

[35] J. Běhal *et al.*, "Toward an all-optical fingerprint of synthetic and natural microplastic fibers by polarization-sensitive holographic microscopy", *ACS Photonics*, vol. 9, no. 2, pp. 694–705, 2022. DOI: 10.1021/acsphotonics.1c01781.

[36] W. Ai, G. Chen, X. Yue, and J. Wang, "Application of hyperspectral and deep learning in farmland soil microplastic detection", *Journal of Hazardous Materials*, vol. 445, art. 130568, 2023. DOI: 10.1016/j.jhazmat.2022.130568.

[37] S. Genc, K. Icoz, and T. Erdem, "Numerical analysis and experimental verification of optical scattering from microplastics", *Royal Society Open Science*, vol. 10, no. 8, 2023. DOI: 10.1098/rsos.230586.

[38] A. Singh *et al.*, "An approach towards different techniques for detection of heavy metal ions and their removal from waste water", *Journal of Environmental Chemical Engineering*, vol. 12, no. 3, art. 113032, 2024. DOI: 10.1016/j.jece.2024.113032.

[39] B. Lin, Z. Xu, J. Wang, and M. Lu, "A low-cost water quality monitoring prototype device with embedded chromogenic reagent capsules and dynamic colorimetric detection", *Sensors and Actuators B: Chemical*, vol. 252, pp. 24–29, 2017. DOI: 10.1016/j.snb.2017.05.056.

[40] J. A. Grant-Jacob *et al.*, "Particle and salinity sensing for the marine environment via deep learning using a Raspberry Pi", *Environmental Reserach Communications*, vol. 1, no. 3, p. 035001, 2019. DOI: 10.1088/2515-7620/ab14c9.

[41] E. Nicolai, R. Pizzoferrato, Y. Li, S. Frattegiani, A. Nucara, and G. Costa, "A new optical method for quantitative detection of microplastics in water based on real-time fluorescence analysis", *Water*, vol. 14, no. 20, p. 3235, 2022. DOI: 10.3390/w14203235.

[42] S. B. Dhal *et al.*, "An IoT-based data-driven real-time monitoring system for control of heavy metals to ensure optimal lettuce growth in hydroponic set-ups", *Sensors*, vol. 23, no. 1, p. 451, 2023. DOI: 10.3390/s23010451.

[43] *AS7265x Datasheet*, ams OSRAM Group, 2018. [Online]. Available: https://look.ams-osram.com/m/76ce4c0d80cd1565/original/AS7265x-DS000612.pdf

[44] E. Frank, M. A. Hall, and I. H. Witten, "The WEKA workbench", in *Data Mining*. Elsevier, 2017, pp. 553–571.